Modeling neuro-immune interactions during Zika virus infection

Pinar Mesci [1,6], Angela Macia[1,6], Christopher N. LaRock[2], Leon Tejwani[1], Isabella R. Fernandes[1], Nicole A. Suarez[1], Paolo M. de A. Zanotto[3], Patricia C. B. Beltrão-Braga[4,5], Victor Nizet[2] & Alysson R. Muotri[1*]

[1]University of California San Diego, School of Medicine, Department of Pediatrics/Rady Children's Hospital San Diego, Department of Cellular & Molecular Medicine, Stem Cell Program, La Jolla, CA 92093-0695, USA.

[2]University of California San Diego, School of Medicine, Department of Pediatrics and Skaggs School of Pharmacy and Pharmaceutical Sciences, La Jolla, CA 92093-0760, USA.

[3]University of São Paulo, Department of Microbiology, Institute of Microbiology Sciences, Laboratory of Molecular Evolution and Bioinformatics, São Paulo, São Paulo 05508-000, Brazil.

[4]University of São Paulo, Department of Surgery, Stem Cell Laboratory, São Paulo, São Paulo, 05508-270, Brazil.

[5]School of Arts Sciences and Humanities, Department of Obstetrics, São Paulo, SP. 03828-000, Brazil.

[6]Co-First Authors.

*To whom correspondence should be addressed: Dr. Alysson R. Muotri, 2880 Torrey Pines Scenic Drive, La Jolla, CA 92093-0695, Email: muotri@ucsd.edu, Phone: (858) 534-9320.

Keywords: Zika, microglia, NPC, hiPSC, Sofosbuvir

Abstract

Although Zika virus (ZIKV) infection is often asymptomatic, in some cases it can lead to birth defects in newborns or serious neurologic complications in adults. However, little is known about the interplay between immune and neural cells that could contribute to the ZIKV pathology. To understand the mechanisms at play during infection and the antiviral immune response, we focused on neural precursor cells (NPC)-microglia interactions. Our data indicate that human microglia infected with the current circulating Brazilian ZIKV induces a similar pro-inflammatory response found in ZIKV-infected human tissues. Importantly, using our model, we show that microglia interact with ZIKV-infected NPCs and further spread the virus. Finally, we show that Sofosbuvir, an FDA-approved drug for Hepatitis C, blocked viral infection in NPCs and therefore the transmission of the virus from microglia to NPCs. Thus, our model provides a new tool for studying neuro-immune interactions and a platform to test new therapeutic drugs.

Introduction

Zika virus (ZIKV) is an arbovirus belonging to the genus *Flavivirus* first described in 1947 in Uganda during blood analyses of sentinel *Rhesus* monkeys (1). Until the 21st century, African and Asian lineages of ZIKV did not cause substantial human infections. However, in 2007, vectored by *Aedes aegypti* mosquitoes, the first noteworthy epidemic of ZIKV occurred on the island of Yap in Micronesia (2). The recent dramatic increase in newborns with microcephaly and other congenital malformations in Brazil has been associated with an outbreak of ZIKV (3, 4). The outbreak has further been linked to the autoimmune neurological disorder Guillain-Barré syndrome (GBS) in older children and adults (5). The circulating Asian-lineage strain of ZIKV in Brazil (ZIKV^{BR}) has been detected in the placenta and amniotic fluid of women with microcephalic fetuses (6–8) and in the blood of microcephalic newborns. Curiously, although the African MR-766 strain of ZIKV (ZIKV^{MR766}, strain MR-766) was first identified in the 1950s, no birth defects in newborns or neurological complications in adults have been associated with this strain. Thus, recent publications focused on the mechanisms of transmission and spreading of ZIKV in the Americas (9–12).

Earlier this year, Liu and colleagues reported that ZIKV evolved to acquire a spontaneous mutation in its NS1 (A188V mutation) domain leading to increased antigenaemia (12). This enhancement of NS1 antigenaemia promoted ZIKV infectivity and prevalence in mosquitoes that could ease the transmission and possibly explain the recent ZIKV outbreaks. Following this publication, another group suggested that the A188V mutation on NS1 domain arose in Southeast Asia at the early 2000s and circulated in that region several years before spreading to South Pacific Islands and the Americas (13) Moreover, there is now converging evidence that the African strains lead to higher infection rate and viral production as well as stronger cell death in cellular and immunocompetent adult mouse models leading to the increased mortality while the

Asian strains did not (14–16). This feature of the Asian strain might be responsible for causing chronic infections observed in congenital microcephaly cases and explain why no other diseases were observed until recently. Hence, there is an urgent need to develop model systems to examine the complex relationship between ZIKV^{BR} infection and brain malformations.

In order to model ZIKV^{BR} infectivity, we previously showed that ZIKV^{BR} crosses the placenta to infect the fetus *in vivo*, causing microcephaly and birth defects (17). In addition, we showed that ZIKV^{BR} targeted human neural precursor cells (NPCs), growing as neurospheres or organoids, induced cell death and led to a reduction of proliferative zones and a disruption of cortical layers as previously observed *in vivo* (17). Despite advances regarding the causal relationship between the ZIKV^{BR} and birth defects, little is known about the pathogenic interactions of this virus with different cell types and its vertical transmission to fetal brain.

Since the onset of the current Brazilian outbreak in 2015, most ZIKV studies have focused on neurons and glial cells (17, 18). However, further examination of ZIKV interaction with fetal circulating monocytes and the interplay between microglia and neural cells are important steps for understanding ZIKV pathophysiology. A recent publication, using the contemporary ZIKV strain PRVABC59 (PR2015), showed that the virus can infect and replicate in Hofbauer cells (HC), a type of primary human placental macrophage (19). Hence, one possibility for intrauterine transmission allowing ZIKV to gain access to the fetal compartment is by direct infection of cells comprising the placental barrier (19). Yolk sac macrophages invade the brain parenchyma through the blood vessels during embryogenesis to become resident macrophages of the central nervous system (CNS), microglia (20). Considering the timing during embryogenesis of the entry of myeloid precursors, we hypothesized that microglia could also actively participate during ZIKV infection, perhaps acting as a Trojan horse by transporting the ZIKV during CNS invasion (21). Thus, in this study, using a ZIKV strain isolated from a clinical case in northeast of Brazil (17), ZIKV^{BR}, we aimed to mimic those early interactions between neural precursor cells (NPC) and macrophage/microglia.

Here, we used human induced pluripotent stem cells (hiPSCs) to model immune interactions in the developing central nervous system of the fetal brain during ZIKV infection by generating human macrophages/microglia and NPCs from the same healthy donor. Then, we established a co-culture system to model the cellular interplay that naturally occurs in the developing human brain. Our data reveal that a similar immune response was elicited in developing human microglia upon infection with the $ZIKV^{BR}$ as was found in the humoral immune response present in ZIKV-infected human tissues (22–25). Upon co-culture, microglia interacted with $ZIKV^{BR}$-infected NPCs. Our data further show that ZIKV-infected macrophages/microglia transmit the virus to naïve NPCs, increasing the apoptosis of NPCs. These results imply that during embryogenesis, myeloid precursors could be responsible for ZIKV transmission to the CNS during their normal process of brain invasion. Finally, we tested Sofosbuvir (SOF), an FDA-approved drug against Hepatitis C infection, previously tested against ZIKV (26–28), and showed that SOF was able to decrease the cell death of ZIKV-infected NPCs. Our findings reveal that human microglia are profoundly influenced by their microenvironment and can sense ZIKV-infected cells in their immediate surroundings, providing insights on the mechanism of infection. Thus, our co-culture system could be used for studying neuro-immune interactions *in vitro* and testing new therapeutic candidates against ZIKV.

Results

Characterization of hiPSC-derived macrophage/microglia (MΦ)

To understand the immune component of neurologic abnormalities observed in ZIKV-infected newborns, we first generated MΦ from human induced pluripotent stem cells (hiPSCs) using an edited version by Douvaras and colleagues of the previously published protocol by Yanagimachi et al., (29, 30) . This serum-free, feeder-free method gave rise to CD14+ monocytes, precursors of MΦ, in suspension starting at 15 days *in vitro*. $CD14^+$ cells were then sorted using magnetic-activated cell sorting (MACS) system, treated with M-CSF and IL-34 for a week as previously published (29), and used in the subsequent experiments (**Fig.S1A**). These monocytes expressed classical MΦ markers such as Iba1 and CD68 (**Fig. 1A**). The analysis of the cells in suspension, prior to CD14 sorting, revealed that they expressed monocyte, macrophage and myeloid cell markers such as CD45/CD14, CD14/HLA-DRDPDQ, CD14/CD11b and CD14/CD68, (**Fig. 1C, Fig.S1B**). One week after sorting, $CD14^+$ cells established a homogeneous macrophage population (**Fig. S1C**) and had similar cellular morphology and expression of cell markers such as CD68 and Iba1 to blood monocyte-derived macrophages (**Fig. S1C-D**). We next assessed whether the MΦ were functional by measuring their capacity for phagocytosis (**Fig. 1B**). In a classical assay (31–33), hiPSC-derived MΦ engulfed the yeast particle zymosan (**Fig. 1B**). The MΦ were also able to phagocytose living cells of the leading neonatal bacterial pathogen group B *Streptococcus* (GBS) whereas hiPSC-derived NPCs or 4 week-old neurons did not internalize the bacterium (**Fig. 1B**); primary human neutrophils were used as positive control of phagocytosis. In addition, we measured cytokine (IL-6, IL-1 β, IL12/IL23p40), chemokine (MIP1 α, MIP1 β, RANTES, Fractalkine, IL8 and IP10) and the growth factor G-CSF release by hiPSC-

derived MΦ after activating them with the classical pro-inflammatory TLR-4 ligand lipopolysaccharide (LPS) using multiplex cytometric bead based-assay (**Fig. 1D, Fig. S1E**). All cytokines/chemokines tested were readily detected in the MΦ conditioned media. LPS treatment for 24 hours significantly increased levels of IL-6, IL-1 β, IL12/IL23p40, Fractalkine, G-CSF, IP10, RANTES, MIP1 α and MIP β (**Fig. 1D, Fig.S1E**).

In sum, hiPSC-derived MΦ displayed monocyte and myeloid markers (**Fig.S1D**), phagocytosed zymosan particles and whole bacteria and responded to a pro-inflammatory stimulus as measured by cytokine/chemokine release similar to primary blood-derived monocytes/macrophages (34).

Immune response of macrophages/microglia (MΦ) upon infection with the ZIKV

Next, we studied the immune response of MΦ upon infection with $ZIKV^{BR}$ as well as with $ZIKV^{MR766}$, a lab-adapted, highly *in vitro* passaged African MR766 strain, presumably different from the circulating African strain at 12 and 24 hours post-infection (p.i) (**Fig S2A-B**). We selected a panel of potential virus entry receptor candidates based on recent publications including *AXL, TIM, TYRO3, MER* and several TLR receptors previously linked to ZIKV and arboviruses such as DENV (32, 33, 39); *TLR3, TLR4, TLR7*, to measure the expression levels by qRT-PCR (17, 18, 35, 36). At 12h p.i., we did not observe any significant changes between the strains when compared to mock-infected samples (**Fig S2A**). At 24 hours p.i., both strains of the virus triggered a *TLR7* up-regulation and only $ZIKV^{MR766}$-infected MΦ expressed higher levels of the *MER* receptor when compared to mock-infected conditions (**Fig. S2B**). Next, we used a lower MOI aiming to mimic the ZIKV infection *in vivo* and to unveil the most sensitive changes without inducing a dramatic inflammatory response that could mask small and strain-specific changes (37–41). Thus, these ranges of MOIs and 24h p.i. time point were used in the subsequent experiments (**Fig. 1E-F**).

TYRO3 and *AXL* were upregulated upon the ZIKV^{BR} infection, with *AXL* gene expression increased by three-fold compared to the mock-infected MΦ (**Fig. 1E**). In contrast, expression of *MER* and *TIM* did not differ between ZIKV^{BR}-infected and mock-infected MΦ (**Fig. 1E**). As for the TLR receptors expression, we focused on three relevant for our study: *TLR3*, a sensor of RNA viruses, which was recently linked to ZIKV infection (35); *TLR4*, which plays a central role in recognition of LPS from Gram-negative bacteria, which was previously shown to be upregulated in ZIKV-infected human neurospheres (36); and *TLR7*, a sensor of ssRNA involved in the detection of other arboviruses such as DENV (42). Surprisingly, all were downregulated when compared with mock-infected controls (**Fig. 1E**). Interestingly, the corresponding changes seen in *AXL*, *TYRO3*, and *TLR7* gene expression upon infection with the ZIKV^{BR} were absent in parallel infections with the ZIKV^{MR766}, which did not differ from mock-infected MΦ in expression of all three receptor genes (**Fig. 1E**).

The geographic and symptomatology overlap between ZIKV and other Flaviviruses such as Dengue (DENV) initially complicated diagnosis (42). The vector by which it is propagated (*Aedes aegypti)* is shared by both viruses and clinically presented serological cross-reactivity. In addition, DENV is known to target primary blood cells such as monocytes and macrophages and induces an inflammatory response (42) . Thus, we next measured the expression of genes encoding three receptors described for DENV infection: *CLEC5A*, *CD209*/DC-SIGN, and *CD206*/MRC1 (**Fig. 1F**). All three viral receptors, *CLEC5A*, *CD209*/DC-SIGN, and *CD206*/MRC1, were downregulated in ZIKV^{BR} or ZIKV^{MR766}-infected MΦ compared to mock-infected MΦ, suggesting that ZIKV does not implicate these DENV-related receptors in iPSCs-derived MΦ (**Fig. 1F**).

Next, we studied the expression of the MΦ markers such as *AIF1*/Iba1, *CD68,* and *ITGAM/*CD11b by qRT-PCR upon infection with the ZIKV strains. *AIF1*/Iba1 expression was increased in the MΦ infected with ZIKV^{BR} compared to the mock-infected or ZIKV^{MR766}-infected

cells, whereas similar changes in *CD68* expression did not achieve statistic significance (**Fig. 1F**). Notably, pro-inflammatory genes encoding *IL6*, *IL1B*, and *CCR5* were markedly induced upon infection by the ZIKV^{BR}, but not ZIKV^{MR766}. In contrast, the MΦ marker *ITGAM*/CD11b and the anti-inflammatory factor *IGF1* were decreased by infections with either ZIKV strain, whereas expression of *CYBB*/NOX2 remained unchanged upon infection with the viruses (**Fig. 1F**). These results indicate that the inflammatory response of MΦ infected with two different ZIKV strains at the same viral MOI elicited different inflammatory responses.

We next compared cytokine/chemokine release by the hiPSC-derived MΦ 24 hour p.i. with the ZIKV^{BR} or ZIKV^{MR766}, (**Fig. 1G** and **Fig. S4**) using the same multiplex cytometric bead array that was used previously (**Fig 1D, FigS1E**). Using several inocula of virus (MOI=0.05, MOI=0.01 and MOI=0.001), we detected changes in release of several pro-inflammatory cytokines/chemokines (**Fig. 1G** and **Fig. S4B-C**). MΦ release of pro-inflammatory cytokines IL12/IL23p40, IL1β, IL10 and the growth factor G-CSF was significantly higher in response to ZIKV^{BR} compared to ZIKV^{MR766} infection; whereas MIP1β, RANTES, IP-10, IL6, and MIP1α release from ZIKV-infected MΦ were comparable between the two strains (**Fig. 1G** and **Fig. S4B-C**), arguing for a ZIKV^{BR}-specific response by the hiPSC-derived MΦ.

Differential expression of TAM/TIM and TLR receptors in human NPCs

Human NPCs were shown to be targeted by ZIKV^{BR} (17). Similar to MΦ, we first infected NPCs at an MOI of 0.1 with either strains and studied the expression of different viral entry receptors at 12 and 24 hours p.i. by qRT-PCR (**Fig.S2C-D**), however, we did not detect any differences between the two different strains at 12h p.i. **(Fig. S2C)**. At 24h p.i., *TYRO3* and *TLR4* were both upregulated in NPCs upon infection with both ZIKV^{BR} and ZIKV^{MR766} strains (**Fig. S2D**). Given that we did not see major differences in gene expression in both of the strains tested, we focused on the same MOI (0.001) determined from the MΦ expression analysis and

the time points (24 and 96 hours p.i.) (**Fig. 1A-B** and **Fig. S2A-B**) for the NPCs (**Fig. S3A-B**). Of four receptors analyzed, only the *MER* was increased in the ZIKV^{BR} 24 hours p.i. compared to mock but returned to mock levels by 96 hours p.i. (**Fig. S3A**). Expression of *TYRO3* was downregulated in both mock- and ZIKV^{BR}-infected NPCs at 96 hours p.i. compared to 24 hours p.i. (**Fig. S3A**). *TLR4* was also decreased as in MΦ, while *TLR7* expression was increased compared to the mock-infected controls at 24hours p.i. (**Fig. S3B**). The expression of TAM/TIM receptors and TLRs observed in NPCs at 96 hours p.i. were accompanied by a decreased expression of cell markers such as *NES*/Nestin and *PAX6* in both mock- and ZIKV^{BR}-infected NPCs (**Fig. S3C**).

To summarize, we did not observe great changes in ZIKV^{BR}-infected NPCs except for *MER* and *TLR7*, which were significantly upregulated compared to the mock-infected NPCs at 24 hour post-infection.

The interplay between NPCs with macrophages/microglia (MΦ) during ZIKV infection

To investigate interactions of hiPSC-derived MΦ with ZIKV^{BR}-infected NPCs we established a co-culture experimental platform. NPCs were infected (MOI = 0.1) for 2 hours with the ZIKV^{BR} or ZIKV^{MR766}, media replaced, and MΦ overlaid 2 hours after the media change. MΦ and NPCs were maintained in co-culture for 96 hours, and the fraction of cells undergoing cell death examined by DNA fragmentation using terminal deoxynucleotidyl transferase dUTP nick end labeling (TUNEL) (**Fig. 2A-B, Fig. S5**). We initially seeded the same amount of MΦ and NPCs, however, the proliferation rate of the NPCs was higher and thus the percentage of MΦ in the co-culture with NPCs was around 2% at 96 hours p.i. (**Fig. S5C**). In the absence of infection, addition of MΦ in co-culture atop NPCs did not influence the number of TUNEL^{+} cells (~ 10%, see **Fig.2C**). However, as previously shown (17), ZIKV^{BR} infection at MOI = 0.1 doubled the percentage of TUNEL^{+} NPCs (**Fig. 2B-C**). No increase in TUNEL^{+} was detected in NPCs

infected with ZIKV^{BR} at MOI = 0.01 for 96 hours (**Fig. S5A**). Infection with ZIKV^{MR766} had similar effect by increasing the amount of TUNEL+ NPCs (**Fig. S5B**). In addition, the amount of MΦ undergoing apoptosis (TUNEL^{+}) remained under ~ 5% in presence or absence of ZIKV^{BR} indicating that the ZIKV^{BR} was not cytotoxic to MΦ under our experimental conditions (**Fig. 2B-C, Fig. S5D**). Interestingly, adding MΦ to ZIKV-infected NPCs reduced the percentage of TUNEL^{+} cell levels similar to mock-infection (**Fig. 2B-C, Fig.S5B**). Thus, while adding naïve MΦ to uninfected NPCs did not increase cell death, infection of NPCs with the ZIKV^{BR} increased cell death, and the presence of MΦ reduced cell death in ZIKV^{BR}-infected NPCs (**Fig. 2B-C**). To elucidate the mechanism by which MΦ presence could decrease TUNEL^{+} ZIKV^{BR}-infected NPCs, whether it is through phagocytosis or through protection by release of neurotrophic factors by MΦ, we used conditioned media (CM) from mock or ZIKV^{BR}- infected MΦ and added on top of NPCs (**Fig. 2D**). Mock MΦ CM did not have any effect on the basal level of apoptosis in mock-infected NPCs whereas ZIKV^{BR} MΦ CM addition tended to increase the level of TUNEL^{+} NPCs (**Fig.2D**). Although the addition of mock or ZIKV^{BR} MΦ CM on top of ZIKV^{BR}-infected NPCs had a small tendency to decrease the amount of TUNEL^{+} cells, there were no statistically significant change compared to ZIKV^{BR}-infected NPCs in the absence of any CM (**Fig. 2D**). Thus, MΦ most likely need to be in contact with NPCs to decrease the amount of TUNEL^{+} NPCs, most likely by phagocytosing the apoptotic cells.

Finally, to assess whether ZIKV-infected MΦ could transmit the virus to the NPCs, we first infected MΦ with ZIKV (ZIKV^{BR} or ZIKV^{MR766}, **Fig. S5**), washed and added on top of NPCs the next day (**Fig.2E**). We co-cultured ZIKV-infected MΦ with NPCs for 96 hours and analyzed the amount of TUNEL^{+} cells (**Fig.2E-F, Fig. S5E**). Importantly, upon addition of ZIKV-infected MΦ on top of NPCs, the amount of TUNEL^{+} cells increased significantly (**Fig.2F-G, Fig.S5E**). Keeping in mind that MΦ represent around 2% of the cells in total (**Fig. S5C**) and that ZIKV

infection did not increase the MΦ in apoptosis (**Fig. S5D**), the increase in TUNEL can be attributed to the increase of cell death of NPCs (**Fig. 2G, Fig. S5E**). More importantly, we tested an FDA-approved drug, Sofosbuvir (SOF), which was previously shown efficient against ZIKV infection in our model (26, 28, 43).

Next, in a following experiment, we added 20 μM SOF at the same time as the addition of ZIKV-infected MΦ on top of uninfected NPCs (**Fig.2E, Fig.2G-H, Fig. S5E-F**). Importantly, addition of SOF decreased significantly the amount of $TUNEL^+$ cells in the case of $ZIKV^{BR}$-infected MΦ addition (**Fig. 2F-G**) and showed a tendency to decrease upon infection with $ZIKV^{MR766}$-infected MΦ (**Fig. S5E**). In addition, this decrease was accompanied by a decrease the amount of the flavivirus $NS1^+$ domain specific staining, suggesting that SOF was able to limit the $ZIKV^{BR}$ replication (**Fig. 2F-H**). As for the MR766, SOF had only a tendency to decrease the amount of $NS1^+$ cells (**Fig.S5F**). Thus, SOF was able to block the increased cell death of NPCs due to the infection by ZIKV-infected MΦ.

Altogether, our model was able to mimic neuro-immune interactions, which is likely to occur during human neurodevelopment and was proven to be useful for testing new therapeutic drugs to block ZIKV-associated phenotypes.

Discussion

In this study, we modeled immune interactions between NPCs and macrophages/microglia (MΦ) that would occur in the developing brains of the ZIKV^{BR}-infected fetuses/newborns, using an induced pluripotent stem cell experimental platform. A fundamental strength of induced pluripotent stem cells is the possibility of deriving different cell types from individuals *in vitro*. Generation of MΦ using this technology will circumvent the need for MHC-matched bone marrow-derived MΦ from a healthy donor. In addition, by generating NPCs and MΦ from the same donor, we established an autologous approach to the study of immune interactions between different cell types derived from the same genetic background. The novelty of our study relies on the establishment of an *in vitro* platform, able to mimic human neuro-immune interactions. In particular, these interactions in human cells were studied by co-culturing hiPSC-derived NPCs together with hiPSC-derived MΦ. To our knowledge this is the first study enabling the analysis of human neuro-immune interactions, unlike the studies using 3D organoids, where the mesoderm-derived immune cells such as MΦ of the central nervous system are lacking, which is a major limitation of this technology (17, 35, 44–46). Thus, we strongly believe that our platform could be further used in other studies implicating MΦ to model the interplay among the different cell types and their impact on neurodevelopmental diseases.

In this study, using low MOI infections to mimic the ZIKV infection *in vivo*, we analyzed the cytokine and immune receptor responses to infections with the ZIKV^{BR} or ZIKV^{MR766} strains. We then investigated cellular receptors implicated in ZIKV cell entry in developing human MΦ, beginning with C-type lectin receptors known to bind DENV on the surface of macrophages and dendritic cells and modulate inflammatory responses (42, 47). Unlike in DENV infections, *CLEC5A*, *CD209*/DC-SIGN and *CD206*/MRC1 all had reduced expression in ZIKV^{BR} and ZIKV^{MR766}-infected MΦ compared to controls (42, 47). TAM/TIM receptors and TLRs have been

recently implicated in ZIKV infection (18, 35). We found that MΦ and NPCs had differential expressions of the genes encoding these receptors upon infection with ZIKV^{BR}: *TYRO3* and *AXL* were upregulated in MΦ infected with ZIKV^{BR} unlike NPC, which had only an upregulation of *MER*, suggesting that AXL does not have a central role in ZIKV infections in NPCs. Indeed, several publications focused on AXL receptors over the last year since it was suggested as a potential viral entry receptor (18), however, two independent studies showed that blocking AXL does not prevent ZIKV infection of NPCs (46, 48). But a recent publication claim that selective expression of Musashi in NPCs could explain their increased vulnerability to ZIKV (49). In the future, experiments such as RNAseq on ZIKV-infected MΦ and NPCs could be more informative to comprehend mechanisms underlying ZIKV-infections. Thus, more research is needed to unveil the different mechanisms underlying ZIKV infection of immune and neural cells.

Regarding TLR receptors, we show that all three TLRs, *TLR3, TLR4* and *TLR7* were downregulated in ZIKV^{BR}-infected MΦ. On closer examination of the inflammatory response, we showed that ZIKV^{BR}-infected MΦ expressed higher levels of *AIF1, IL6, IL1β* and *CCR5* and released higher levels of IL12/IL23p40, IL1β, IL10 and G-CSF upon infection with ZIKV^{BR} but not with ZIKV^{MR766} suggesting that the Brazilian strain might induce a distinct inflammatory response at lower MOIs. In line with this, a recent publication showed that the Asian-lineage ZIKV infection of pregnant women's blood led CD14^{+} monocytes to a M2 phenotype, with a notable increase in IL-10 production (50), suggesting that our ZIKV^{BR}-infected MΦ can, at least partially, recapitulate the strain-specific features of ZIKV infection. Noteworthy, as stated previously, the African strain MR766 of the ZIKV has been passaged multiple times *in vitro*, hence the differences seen in inflammatory response could be attributed to the artificial nature of MR-766 strain (51). Thus, this platform could be used to distinguish subtle differences between the several viruses.

Interestingly, Manangeeswaran and colleagues found increased levels of IL1β in the CNS of IFNAR KO mice upon infection with an Asian strain of the ZIKV (24). Another study investigating

the cytokine kinetics upon ZIKV infection of travelers from Thailand, Tahiti, Malaysia and Brazil, found also elevated levels of IL1β and IL10 in the blood (23). A Brazilian patient who developed with encephalomyelitis upon ZIKV infection, showed elevated levels of G-CSF in the cerebrospinal fluid (25). Finally, a recent study that evaluated the humoral response during ZIKV infection in the amniotic fluid of ZIKV-positive pregnant women with neonatal microcephaly reported elevated IP-10, IL6, IL8, MCP-1 and G-CSF (22). Altogether, we show that the Brazilian Zika virus induced similar inflammatory response by hiPSC-derived MΦ, thus resembling the immune activation observed in patients, including pregnant women infected with ZIKV. Therefore, hiPSC-derived MΦ could be used as potential targets for drug development.

Finally, in order to mimic the immune interactions occurring between macrophages of the central nervous system, microglia, and NPCs in the fetal brain during ZIKV infection, we derived hiPSC-derived MΦ and NPCs from the same donor. We then established a co-culture system to study the multi-cellular interactions that will occur during infection, such as between naïve MΦ and $ZIKV^{BR}$-infected NPCs. In our co-culture system, we sought to mimic the microglia percentage *in vivo* which in mouse cortex is around 5% (52–55). In our experiments, we obtained 2% MΦ after 96 hours of co-culture both in $ZIKV^{BR}$ or mock-infection conditions, similar to the percentage of microglia found *in vivo* (52–55). When we added naïve MΦ to infected NPCs, the percentage of dying NPCs decreased significantly. Moreover, by using conditioned media from mock or $ZIKV^{BR}$-infected MΦ, we explained our results mechanistically by identifying MΦ phagocytosis of apoptotic NPCs, demonstrating that hiPSC-derived MΦ are functional in their ability to recognize virus-infected cells. Furthermore, we showed that conditioned media from $ZIKV^{BR}$-infected MΦ alone is not sufficient to cause apoptosis of NPCs in our experimental conditions and that physical contact is necessary. The MΦ inflammatory response to ZIKV

infection together with the phagocytosis of ZIKV-infected NPCs by MΦ, could contribute to microcephaly in newborns.

Next, we hypothesized that ZIKV-infected MΦ could transmit the virus to the NPCs since the timing of microglial CNS invasion during neurodevelopment corresponds to the timing of ZIKV antigen detection in placental tissues (20, 56). Indeed, our data show that ZIKV-infected MΦ transmit ZIKV to NPCs, increasing apoptosis. Importantly, an FDA-approved drug, SOF, was able to block the cell death of NPCs in this context.

Finally, one of the classic pathological findings in GBS, which has been linked to the Zika virus outbreak (5), is inflammatory infiltrates, mainly T cells and macrophages (57). Thus, our *in vitro* model using hiPSC-derived MΦ could be used to further investigate the inflammatory machinery involved in GBS. Our study sheds light on the immune implications of ZIKV infection and might give insights on the risk of developing ZIKV-associated GBS. Thus, we propose that MΦ could be a therapeutic target to limit the virus spreading amongst the most vulnerable and relevant cell types involved in microcephaly, such as NPCs, and that our co-culture model could be used for drug discovery against ZIKV infection.

Experimental Procedures:

Cell Culture

hiPSC-derived macrophages/microglia (MΦ) differentiation protocol was adapted from (29) and (30). Briefly, iPSCs cell lines were generated as previously described, by reprogramming fibroblast from two healthy donors (58). The iPSC colonies were plated on Matrigel-coated (BD Biosciences) plates and maintained in mTESR media (Stem Cell Technologies). The protocol of myeloid cell lineage consisted of 4 sequential steps. In the first step, primitive streak cells were induced by BMP4 addition, which in step 2, were differentiated into hemangioblast-like hematopoietic precursors [VEGF (80 ng/ml, Peprotech), SCF (100 ng/ml, Gemini) and basic fibroblast growth factor (bFGF), (25 ng/ml, Life Technologies)]. Then, in the third step, the hematopoietic precursors were pushed towards myeloid differentiation [FLT-3 ligand (50 ng/ml, HumanZyme), IL-3 (50 ng/ml, Gemini), SCF (50 ng/ml, Gemini), Thrombopoietin, TPO (5 ng/ml), M-CSF (50 ng/ml)] and finally into the monocytic lineage in step 4 [FLT3-ligand (50 ng/ml), M-CSF (50ng/ml), GM-CSF (25 ng/ml)]. Cells produced in suspension in step 4 were recovered, sorted by using anti-CD14 magnetic microbeads (MACS, Miltenyi), treated with 50ng/ml M-CSF and 50ng/ml IL-34 for a week before being used in different experiments.

Monocyte-derived macrophages were isolated from the peripheral blood of a healthy donor as previously described (34). PBMCs were isolated from the blood by density gradient centrifugation. $CD14^+$ monocytes were then purified by MACS using CD14 microbeads.

For the generation of NPCs, cell were differentiated and maintained as previously described (58–60). Two iPSCs lines obtained from healthy patients maintained in mTSER media were switched to N2 [DMEM/F12 media supplemented with 1xN2 NeuroPlex Serum-Free

Supplement (Gemini) with the dual SMAD inhibitors 1 μ M of dorsomorphin (Tocris) and 10uM of SB431542 (Stemgent) daily, for 48 hours. After two days, colonies were scraped off and cultured under agitation (95rpm) as embryoid bodies for seven days using N2 media with dorsomorphin and SB431542. Media was changed every other day. Embryoid bodies were then plated on Matrigel-coated dishes, and maintained in DMEM/F12 supplemented with 0.5x of N2 supplement, 0.5x Gem21 NeuroPlex Serum-Free Supplement (Gemini), 20 ng/mL basic fibroblast growth factor (bFGF, LifeTechnologies) and 1% penicillin/streptomycin (P/S). After 7 days in culture, rosettes that arose from the plated EBs were manually selected, gently dissociated with StemPro Accutase (LifeTechnologies) and plated onto 10 µg/mL poly-L-ornithine (Sigma)/ 5 µg/mL Laminin (LifeTechnologies) coated plates. Neuronal precursor cells (NPCs) were maintained in DMEM/F12 with N2, Gem21, bFGF and P/S. The media was changed every other day. NPCs were split as soon as confluent, using StemPro Accutase for 5min at 37ºC, centrifuged and replated with NGF with a 1:3 ratio in poly-L-ornithine /Laminin-coated plates.

Virus culture and amplification

Both $ZIKV^{BR}$ and $ZIKV^{MR766}$ were obtained and amplified as in (17): lyophilized $ZIKV^{BR}$, which was isolated from a clinical case in Brazil, was provided by the Evandro Chagas Institute in Belém, Pará and was reconstituted in 0.5 ml of sterile DEPC water. The African-lineage MR-766 ($ZIKV^{MR766}$), a reference strain isolated in Uganda in 1947, used here as a control, was provided by the Institute Pasteur in Dakar, Senegal. C6/36 Aedes albopictus mosquito cells were used to culture both viruses. The culture medium used for C6/36 cells was Leibovitz's L-15 medium supplemented with 10% fetal bovine serum (FBS) (Gemini), 1% non-essential amino acids (Gibco), 1% sodium pyruvate (Gibco), 1% penicillin/streptomycine (Gibco) and 0.05% amphotericin B (Gibco). The cells were kept at 27 °C. When cells reached around 70% of

confluency, 50µl of viral sample was added. The cells were subcultured three times before the supernatant was harvested, titrated and used for experimental inoculation.

Virus titration

The virus titration was performed as previously described (17). Briefly, porcine kidney epithelial (PS) cells were used for virus titration in L15 medium with 5% FBS. Serial dilution ranging from 10^{-1} to 10^{-11} for each virus stock were added onto 24-well plates, followed by PS cells seeding into each well of a 24-well plate for 3 hours at 37 °C. Next, each well was overlaid with complete carboxymethyl cellulose medium (0.6% in L15 supplemented with 3% FBS). Following 5 days of incubation in 37 °C, the plaque assay was performed using 0.05% crystal violet solution. The viral dilution was estimated to determine the amount of infected cells (plaque forming units or $PFU.ml^{-1}$).

***In vitro* infection**

NPCs were infected with commercially available $ZIKV^{MR766}$ (MR-766, obtained from ATCC) and $ZIKV^{BR}$, which was isolated from a febrile case in the state of Paraiba (Brazil-ZKV2015) as previously described (17). Briefly, NPCs were seeded in 24-well, infected at different MOIs for an hour at 37°C, then were washed and their media was changed. For NPC and MΦ, both of the viruses were used at MOIs of 0.001 for RNA, 0.001, 0.01 and 0.05 for CBA experiments, 0.1 for the first co-culture experiment and MOI of 1 for the second co-culture experiment.

Cytometric Bead Array (CBA)

The bead-based immunoassay was performed following manufacturer's instructions (BD Biosciences). Briefly, iPSCs-derived MΦ or monocyte-derived macrophages were seeded at a density of $5x10^4$ cells/well. Media was conditioned with or without 1µg/ml lipopolysaccharides

(LPS, Sigma Aldrich) for 24-30hours. 50µl of conditioned media per sample were analyzed by CBA. A customized array of cytokines and chemokines were measured in the conditioned media, including IL1β, IL-6, IL-8, IL-10, IL12/23p40, G-CSF, IP10, sCD14, RANTES, Fractalkine, MIP1α, MIP1β and MCP1, using a BD fluorescence activated cell sorting (FACS) Canto II instrument followed by an analysis on FCAP Array software (BD Biosciences).

Phagocytosis assay

For internalization experiments, hiPSCs-derived MΦ were seeded to 2 x10^4 cells per well. Human neutrophils (PMNs), used as positive controls, were isolated from healthy donors using PolyMorphPrep (Axis-Shield) in accordance with the University of California, San Diego, (UCSD) Human Research Protections Program, and seeded to 2 x10^4 cells per well.
Group B Streptococcus (GBS) strain COH1 was grown overnight at 37°C in Todd-Hewitt broth (Difco), diluted in PBS to MOI=10, and spun onto cell 167 g for 3 minutes. After 90 minutes, the media was supplemented with 100µg/mL gentamicin to kill extracellular bacteria. After 30 minutes, the cells were washed 1x in PBS and lysed with 0.05% Triton-X100 (Sigma) for dilution plating and CFU enumeration on Todd-Hewitt agar plates (Difco).

Co-culture assay

For the first co-culture experiment, 2 x 10^4 NPCs per well of a 96-well plate were plated 24 hours prior to the ZIKV infection. After ZIKV infection for an hour at 37°C, cells were washed and fresh media was added. Two hours later, 2 x 10^4 naïve hiPSCs-derived MΦ per well were plated on top of the NPCs. Cells were fixed 96 hours post-infection for further analysis with 4% paraformaldehyde, for 20 minutes at room temperature. For the second co-culture experiment, 2 x 10^4 NPCs were plated. MΦ were infected at an MOI of 1 for an hour at 37°C and the media was changed. The next day, MΦ were lifted off by adding accutase for 5 minutes, washed with

PBS and centrifuged at 300g for 5 minutes. The cells were counted and $2x10^4$ cells/well of MΦ were added onto NPCs with 20μM of SOF (Acme Bioscience AB3793) or vehicle (DMSO). The dose of 20μM of SOF used on NPCs was optimized in our laboratory (Mesci et al., manuscript in revision). The cells were fixed after 96h of incubation. For mock controls, the same volume of supernatant was added to each experiment.

Imaging analyses

Cells were fixed with 4% paraformaldehyde for 20 minutes at room temperature. Next, samples were permeabilized in 1x-PBS containing 0.1% (v/v) Triton X-100 for 10 minutes. Cells were next incubated with blocking solution [1% fetal bovine serum, (Life Technologies) in 1xPBS]. After 1 hour, the primary antibody was added (diluted in blocking solution) and samples were incubated overnight at 4°C. Slides were then washed two times with 1x-PBS, and incubated with the secondary antibody for 30 minutes at 4°C. Secondary antibodies (all conjugated to Alexa Fluor 488, 555 and 647) were purchased from Life Technologies and used at a 1:1000 dilution. After the 30 minutes incubation, samples were washed twice (1x-PBS), incubated for 5 minutes with and fluorescent nuclear DAPI stain, and mounted with Prolong gold anti-fade reagent (Life Technologies). Samples were imaged using an Axio Observer Z1 Microscope with ApoTome (Zeiss). Captured images were analyzed with Zen software from Zeiss. Antibodies and dilutions used: Monoclonal Mouse Anti-Human CD68, (1:500, Dako); Polyclonal Rabbit Anti-Iba-1, (1:500, Wako). For TUNEL analysis, NPCs were plated, infected after 24 hours, and fixed 96 hours p.i with 4% paraformaldehyde for 20 minutes. Samples were permeabilized with 0.25% Triton X-100 for 15 minutes, and stained for fragmented DNA using TUNEL (Click-iT TUNEL 647 assay kit from Life Technologies). The cells were then blocked 1% bovine serum albumin for 60 minutes. Cells were incubated in primary antibodies: Monoclonal Mouse Nestin, Polyclonal anti-Chicken or Polyclonal Rabbit Nestin (1:500, Abcam); Polyclonal Rabbit Anti-Iba-1, (1:500, Wako) and

monoclonal mouse NS1 (1:250, Millipore) overnight at 4°C and stained with secondary antibodies conjugated to Alexa Fluor and DAPI the following day prior to mounting. Images were blindly collected using an Axio Observer Z1 Microscope with ApoTome (Zeiss) and blindly analyzed with ImageJ software.

Fluorescence-activated cell sorting analyses

Using previously mentioned protocol to generate monocytes/macrophages (29), we have collected the cells in the supernatant at the step 4 and labeled them with the appropriate antibodies (CD45 BV786, CD14 PE, CD11b APC, CD68 PE-Cy7, HLA-DRDPDQ FITC all from BD Biosciences). Briefly, cells were harvested and counted, then washed twice with the stain buffer, containing PBS and 1% heat inactivated FBS, at 300g for 5 minutes. The antibodies were added in the cell mixture and incubated in RT in the dark for 20-30 minutes. The cells were then washed twice with the stain buffer. The cells were resuspended in 500 µl stain buffer and the viability dye, 7-AAD was added. The data was acquired in BD LSRFORTESSA instrument and the plots were generated using the software FlowJo.

RNA extraction and expression analyses by qPCR

Total RNA was extracted from cells using RNeasy Micro and Mini kit for iPSC-derived MΦ and NPCs respectively (Qiagen), following manufacter's instructions. Next, 900 ng of total RNA was treated RNase-free DNaseI (Qiagen), and was reverse transcribed using QuantiTect Reverse Transcription Kit (Qiagen). Approximately 15 ng of cDNAs were used per reaction and PCRs were carried out in a final volume of 10 µl. Triplicate samples were analyzed in a CFX384 Touch Real-Time PCR Detection System (Bio-rad) using iQ™ SYBR® Green Supermix (Bio-rad). GADPH was used as internal normalization control. For the complete list of primers, please refer

to Table 1. The run method was as follows: 3min at 95ºC, 40 cycles of 10s at 95ºC followed by 30s at 58ºC, and a melting curve was performed to confirm the identity of the amplified product.

Statistical analysis

One-way ANOVA or two-way ANOVA (if two or more variables) tests followed by a Tukey or Sidak multiple comparison tests were used to compare groups and Student's t-test to compare means of two groups.

Table 1: List of primers

AXL-F	GTTTGGAGCTGTGATGGAAGGC
AXL-R	CGCTTCACTCAGGAAATCCTCC
CCR5-F	CCTGCTGCTTTGCCTACATTGC
CCR5-R	ACACACTTGGCGGTTCTTTCGG
CD11b-F	GGAACGCCATTGTCTGCTTTCG
CD11b-R	ATGCTGAGGTCATCCTGGCAGA
CD206-F	AGCCAACACCAGCTCCTCAAGA
CD206-R	CAAAACGCTCGCGCATTGTCCA
CD209-F	GCAGTCTTCCAGAAGTAACCGC
CD209-R	GCTCTCCTCTGTTCCAATACTGC
CD68-F	CGAGCATCATTCTTTCACCAGCT
CD68-R	ATGAGAGGCAGCAAGATGGACC
CLEC5A-F	TTGTCAACACGCCAGAGAAACTG
CLEC5A-R	CAACGCCACCTTTTCTCTTCACG
IBA1-F	CCCTCCAAACTGGAAGGCTTCA
IBA1-R	CTTTAGCTCTAGGTGAGTCTTGG
IGF1-F	CTCTTCAGTTCGTGTGTGGAGAC
IGF1-R	CAGCCTCCTTAGATCACAGCTC
IL1B-F	CCACAGACCTTCCAGGAGAATG
IL1B-R	GTGCAGTTCAGTGATCGTACAGG
IL6-F	AGACAGCCACTCACCTCTTCAG
IL6-R	TTCTGCCAGTGCCTCTTTGCTG
MCP1-F	AGAATCACCAGCAGCAAGTGTCC
MCP1-R	TCCTGAACCCACTTCTGCTTGG

MERTK-F	CAGGAAGATGGGACCTCTCTGA
MERTK-R	GGCTGAAGTCTTTCATGCACGC
NOX2-F	CTCTGAACTTGGAGACAGGCAAA
NOX2-R	CACAGCGTGATGACAACTCCAG
TIM-F	CTTCACCTCAGCCAGCAGAAAC
TIM-R	GCCATCTGAAGACTCTGTCACG
TLR3-F	GCGCTAAAAAGTGAAGAACTGGAT
TLR3-R	GCTGGACATTGTTCAGAAAGAGG
TLR4-F	CCCTGAGGCATTTAGGCAGCTA
TLR4-R	AGGTAGAGAGGTGGCTTAGGCT
TLR7-F	CTTTGGACCTCAGCCACAACCA
TLR7-R	CGCAACTGGAAGGCATCTTGTAG
TYRO3-F	GCAAGCCTTTGACAGTGTCATGG
TYRO3-R	GTTCATCGCTGATGCCCAAGCT
NES-F	CCATAGAGGGCAAAGTGGTAA
NES-R	TTCTTCCCATATTTCCTGCTGC
PAX-F	TGTCCAACGGATGTGTGAGTA
PAX-R	CAGTCTCGTAATACCTGCCCA
GAPDH-F	TGCACCACCAACTGCTTAGC
GAPDH-R	GGCATGGACTGTGGTCATGAG

Funding

This work was supported by grants from the California Institute for Regenerative Medicine (DISC2-09649), the National Institutes of Health through the U19MH107367, Zika Network FAPESP projects 2011/18703-2 and 2014/17766-9, the NGO “the tooth fairy project”, a fellowship from the A.P. Giannini Foundation to C.N.L., and an NARSAD Independent Investigator Grant to A.R.M. Dr. Mesci has an International Rett syndrome foundation (IRSF) mentored training fellowship. Dr. Macia has a NARSAD Young Investigator grant.

Acknowledgments

We would like to thank Dr. Edison Durigon and his group for the $ZIKV^{BR}$ aliquots, the UCSD stem cell core and Dr. Christopher Alfonso from BD Biosciences. We would like to thank Spencer M. Moore for critical reading of the manuscript.

Conflict of Interest

The authors declare no conflict of interest.

Authors’ contributions:

P.M., A.M. and A.R.M. directed and designed the study. P.M. developed the hiPSC-derived macrophages/microglia and the co-culture experiments. P.M. and A.M. performed and analyzed all the experiments with the help from C.N.L, V.N. L.T. I.R.F., N.A.S., V.C., P.M.A.Z, P.C.B.B.B and P.M. wrote the manuscript with the input from A.M. and A.R.M.

Figure legends:

Figure 1 | Characterization of functional human induced pluripotent stem cell (hiPSC)- derived macrophages/microglia (MΦ) and their Innate immune system receptors and inflammatory response upon Zika virus (ZIKV) infection.

A. Representative images of hiPSC-derived MΦ stained with anti-Iba1 (green), anti-CD68 (red) and fluorescent nuclear DAPI stain (blue): control MΦ untreated CTRL, (left panel) and treated with lipopolysaccharides (LPS, 100 ng/ml, right panel). Scale bar: 20 μm. **B.** The panel shows pHrodo red zymosan (orange) particles engulfed by hiPSC-derived MΦ, stained with anti-Iba1 (green). Scale bar: 50 μm. Phagocytosis percentage determined by group B streptococcus (GBS) internalization. Note that hiPSC-derived neural precursors (NPC) or neurons do not engulf any GBS. Human primary polymorphonuclear neutrophils (PMN) were used as an experimental positive control. One-way ANOVA with Tukey multiple comparison tests were performed, bars represent means of the percentage of phagocytosis ± SD ***p<0.001. **C.** Fluorescent activated cell-sorting (FACS) analysis of monocytic lineage cells derived sequentially from pluripotent stem cells. **D.** Cytometric Bead Array (CBA) performed on conditioned media from control or 1 μg/ml LPS-treated MΦ for 24-30 hours. Student's t-tests were performed to compare the two groups. Bars represent means of the amount of cytokines/chemokines released in the media (pg/ml) ± SD, *p<0.05, **p<0.01, ****p<0.0001 compared to control (CTRL) untreated cells. **E.** The expression of a panel of potential Zika virus entry receptors including *AXL, TIM, TYRO3, MER* and several TLR receptors (*TLR3, TLR4, TLR7*) was measured by qRT-PCR in MΦ infected with either Brazilian ($ZIKV^{BR)}$ or the highly *in vitro* passaged MR766 ZIKV strain ($ZIKV^{MR766}$) (MOI=0.001). RNA was analyzed 24 hours p.i. One-way ANOVA with Tukey multiple comparison tests were performed. The bars represent means of the mRNA fold change compared to the mock-infected MΦ, shown by a dashed line on the y-axis at 1 ± SD, *p<0.05, **p<0.01, ***p<0.001. **F.** Inflammatory response was measured by qRT-PCR in hiPSC- MΦ infected with

either the ZIKV^{BR} or ZIKV^{MR766} (MOI=0.001). RNA was extracted 24 hours after infection. One-way ANOVA with Tukey multiple comparison tests were performed, bars represent means of the mRNA fold change compared to the mock-infected MΦ, shown by a dashed line on the y-axis at 1 ± SD, *p<0.05, **p<0.01, ***p<0.001, MΦ ZIKV^{BR} is represented in light grey and ZIKV^{MR766} in dark grey. **G**. Inflammatory cytokines/chemokines were measured in the media conditioned by MΦ for 24-30 hours p.i (MOI=0.05) with ZIKV^{BR} or ZIKV ^{MR766}. One-way ANOVA with Sidak multiple comparisons tests were performed. Bars represent average of fold change (in %) compared to the mock-infected MΦ (as shown by the dashed line at 100%) ± SD, *p<0.05, **p<0.01, ****p<0.0001, MΦ ZIKV^{BR} is represented in light grey and ZIKV^{MR766} in dark grey.

Figure 2 | **The impact of ZIKV on macrophage/microglia (MΦ) and NPCs co-culture.**

A. Schematic of the experimental design. ZIKV-infected NPCs are co-cultured with either naïve MΦ or mock or ZIKV^{BR}-infected MΦ-conditioned media (MΦ CM) followed by an analysis of cell death measured by the percentage of TUNEL positive cells. **B.** Images of mock and ZIKV^{BR}-infected NPCs stained with Nestin (green), TUNEL (pink) and fluorescent nuclear staining, DAPI (blue), and MΦ stained with Iba1 (orange) in control (upper left panel), ZIKV^{BR}-infected NPCs (bottom left panel), in control NPCs co-cultured MΦ (upper right panel) and in ZIKV^{BR}-infected NPCs co-cultured with MΦ (bottom right panel). White arrows point to MΦ (orange). Scale bar: 20 μm. **C**. TUNEL images of NPCs infected with the ZIKV^{BR} (MOI =0.1) were acquired, and the percentages of dying cells were calculated, averaged, and graphed accordingly. One-way ANOVA tests with Tukey multiple comparison were performed to compare different groups. The presented values are means of TUNEL^{+}/DAPI^{+} percentage ± SD, **p<0.01, ***p<0.001. Note that infected NPCs have increased TUNEL^{+}/DAPI^{+} percentage compared to the mock and the addition of MΦ decreases TUNEL^{+}/DAPI^{+} percentage. **D.** TUNEL images of NPCs

infected with the ZIKV^{BR} and treated with mock or ZIKV^{BR}-infected MΦ conditioned media (MΦ CM) (MOI=0.1) were acquired, and the percentages of apoptotic cells were calculated, averaged, and graphed accordingly. One-way ANOVA with Tukey multiple comparisons tests were performed to compare different groups. The presented values are means of TUNEL^{+}/DAPI^{+} percentage ± SD, *p<0.05, **p<0.01. **E.** Schematic of the experimental design: ZIKV-infected MΦ are co-cultured with NPCs, treated with either vehicle (VEH) or Sofosbuvir (SOF) for 96 hours before quantification of TUNEL and NS1 positive cells. **F.** Images of ZIKV^{BR}-infected cells stained with Nestin (green), TUNEL (pink), Iba1 (orange) and DAPI (blue) (upper panels), and images of ZIKV^{BR}-infected cells stained with Nestin (green), NS1 (white) and Iba1 (orange) (lower panels). MΦ were treated with either VEH (left panels), or 20μM SOF (right panels) after ZIKV-infection and co-cultured with NPCs. White arrows point to MΦ (orange). Scale bar: 20 μm. **G**. TUNEL images of cells infected with the ZIKV^{BR} (MOI =1) were acquired, and the percentages of dying cells were calculated, averaged, and graphed accordingly. One-way ANOVA tests with Tukey multiple comparison were performed to compare different groups. The presented values are means of TUNEL^{+}/DAPI^{+} percentage ± SD, **p<0.01, ***p<0.001. Note that MΦ treated with SOF and co-cultured infected NPCs have decreased TUNEL^{+}/DAPI^{+} percentage compared to the vehicle (VEH). **H.** NS1 images were acquired, and the percentages of NS1 positive cells were calculated, averaged, and graphed accordingly. One-way ANOVA with Tukey multiple comparisons tests were performed to compare different groups. The presented values are means of NS1^{+}/DAPI^{+} percentage ± SD, *p<0.05.

Figure S1 | Generation and characterization of functional human induced pluripotent stem cell (hiPSC)- derived macrophages/microglia (MΦ).

A. hiPSC-derived macrophage differentiation protocol (Adapted from Yanagimachi et al., 2013 and Douvaras et al., 2017). **B.** Fluorescent activated cell-sorting (FACS) analysis of

monocytic lineage cells derived sequentially from pluripotent stem cells showing CD14/HLA-DR-DP-DQ and CD14/CD68 plots. **C.** hiPSC-derived macrophage differentiated from two different healthy donors. Cells were labeled with anti-Iba1 and anti-CD68 antibodies. Left panel taken at an x20 objective (scale bar: 50µm) and middle and right panel pictures are taken at an x10 objective showing a homogenous population: all $DAPI^+$ cells are also $Iba1^+$(scale bar: 100µm). **D**. Images from primary blood monocyte-derived macrophages and hiPSC-derived macrophages labeled with anti-Iba1 and anti-CD68 antibodies showing similar morphology and cell marker protein expression (scale bar: 50µm). **E.** Cytometric Bead Array (CBA) performed on conditioned media from control or 1 µg/ml LPS-treated MΦ for 24-30 hours. Student's t-tests were performed to compare the two groups. Bars represent means of the amount of cytokines/chemokines released in the media (pg/ml) ± SD, *p<0.05, **p<0.01, ****p<0.0001 compared to control (CTRL), untreated cells.

Figure S2 | Differential expression of TAM/TIM receptors and toll-like receptors (TLR) in hiPSC-derived macrophages/microglia (MΦ) and neural precursor cells (NPC) infected with ZIKV. A-B. The expression of TAM/TIM receptors (*AXL, TIM, TYRO3,* and *MER*) and toll-like receptors (*TLR3, TLR4* and *TLR7)* was measured by qRT-PCR in MΦ 12 and 24 hours p.i. (MOI=0.1). Student's t-test was performed compared to the mock-infected MΦ. Bars represent average of fold change compared to the mock-infected MΦ (represented by a dashed line) ± SD, *p<0.05, **p<0.01, ***p<0.001, ****p<0.0001. **C-D.** The expression of TAM/TIM receptors (*AXL, TIM, TYRO3,* and *MER*) and toll-like receptors (*TLR3, TLR4* and *TLR7)* was measured by qRT-PCR in NPCs 12 and 24 hours p.i. (MOI=0.1) respectively, Student's t-test was performed. Bars represent average of fold change compared to the mock-infected NPCs (represented by a dashed line) ± SD, *p<0.05, **p<0.01, ***p<0.001, ****p<0.0001.

Figure S3 | **Differential expression of TAM/TIM receptors and toll-like receptors (TLR) in hiPSC-derived neural precursor cells (NPC) after 24 and 96 hours of ZIKV^{BR} exposure (MOI=0.001). A.** Expression of TAM/TIM receptors in hiPSC-derived NPCs measured by qRT-PCR. Two-way ANOVA with Sidak multiple comparisons tests were performed. RNA was extracted from NPCs, 24 and 96 hours p.i with the ZIKV^{BR} (MOI = 0.001). Dots represent average of fold change compared to the 24 hours mock-infected NPCs ± SD, *p<0.05, **p<0.01, ***p<0.001. **B**. Expression of toll-like receptors, *TLR3, TLR4* and *TLR7* was measured by qRT-PCR in hiPSC-derived NPCs. RNA was extracted from NPCs, 24 and 96 hours p.i with the ZIKV^{BR} (MOI = 0.001). Two-way ANOVA with Sidak multiple comparisons tests were performed. Dots represent means of fold change compared to mock-infected NPCs ± SD, *p<0.05, **p<0.01, ***p<0.001. **C**. Expression of *NES*/Nestin and *PAX6* was measured by qRT-PCR in hiPSC-derived NPCs. RNA was extracted from NPCs, 24 and 96 hours p.i with the ZIKV^{BR} (MOI=0.001). Two-way ANOVA with Sidak multiple comparisons tests were performed. Dots represent means of fold change compared to mock-infected NPCs ± SD, **p<0.01, ***p<0.001.

Figure S4 | **Cytokine and chemokine release of hiPSC-derived macrophages/microglia (MΦ) infected with ZIKV^{BR} and ZIKV^{MR766} strains, MOI=0.01 and MOI=0.001. A.** Representative image of immunostainings against the MΦ markers CD68 (green) and Iba (orange), and fluorescent nuclear marker DAPI (blue) of mock-infected MΦ (left panel) and ZIKV^{BR}-infected cells (right panel). Scale bar: 20 µm. **B-C**. Inflammatory cytokines/chemokines were measured in the hiPSCs-derived MΦ conditioned media, 24 hours p.i (MOI = 0.01 and 0.001 respectively). One-way ANOVA with Sidak multiple comparisons tests were performed. Bars represent average of fold change (in %) compared to the mock-infected MΦ ± SD, *p<0.01, ****p<0.001.

Figure S5 | The impact of macrophages/microglia (MΦ) on ZIKV^{BR}-infected NPCs.

A. TUNEL images of NPCs infected with the ZIKV^{BR} (MOI =0.1 and MOI=0.01) were acquired, and the percentages of dying cells were calculated, averaged, and graphed accordingly. One-way ANOVA tests with Tukey multiple comparison were performed to compare different groups. The presented values are means of TUNEL^{+}/DAPI^{+} percentage ± SD, *p<0.05. **B.** TUNEL images of NPCs infected with the ZIKV^{MR766} (MOI =0.1) were acquired, and the percentages of dying cells were calculated, averaged, and graphed accordingly. One-way ANOVA tests with Tukey multiple comparison were performed to compare different groups. The presented values are means of TUNEL^{+}/DAPI^{+} percentage ± SD, **p<0.01, ****p<0.0001. Note that infected NPCs have increased TUNEL^{+}/DAPI^{+} percentage compared to the mock and the addition of MΦ significantly decreases TUNEL^{+}/DAPI^{+} percentage. **C**. Percentage of MΦ in the co-culture system. Images with Iba1^{+} cells and DAPI were acquired, counted and the percentage of Iba1^{+} cells was calculated in mock or ZIKV^{BR}-infected conditions. Student's t-tests were performed. **D**. Percentage of TUNEL^{+} Iba1^{+} cells in the co-culture system. Images with Iba1+ cells, TUNEL and DAPI were acquired, counted and the percentage of Iba1+/TUNEL^{+} over the total amount of Iba1^{+} cells was calculated in mock or ZIKV^{BR}-infected conditions. Student's t-tests were performed. **E**. TUNEL images of NPCs infected with the ZIKV^{MR766} (MOI =1) were acquired, and the percentages of dying cells were calculated, averaged, and graphed accordingly. One-way ANOVA tests with Tukey multiple comparison were performed to compare different groups. The presented values are means of TUNEL^{+}/DAPI^{+} percentage ± SD, **p<0.01, ***p<0.001. Note that ZIKV- infected MΦ co-culture with NPCs in the presence of SOF decreased TUNEL^{+}/DAPI^{+} percentage compared to the vehicle VEH treatment. **F.** NS1 images were acquired, and the percentages of NS1 positive cells were calculated, averaged, and graphed accordingly. One-way ANOVA with Tukey multiple comparisons tests were performed to compare different groups. The presented values are means of NS1^{+}/DAPI^{+} percentage ± SD.

References

1. DICK,G.W.A., KITCHEN,S.F. and HADDOW,A.J. (1952) Zika virus. I. Isolations and serological specificity. *Trans. R. Soc. Trop. Med. Hyg.*, **46**, 509–520.
2. Lanciotti,R.S., Kosoy,O.L., Laven,J.J., Velez,J.O., Lambert,A.J., Johnson,A.J., Stanfield,S.M. and Duffy,M.R. (2008) Genetic and serologic properties of Zika virus associated with an epidemic, Yap State, Micronesia, 2007. *Emerg. Infect. Dis.*, **14**, 1232–1239.
3. Campos,G.S., Bandeira,A.C. and Sardi,S.I. (2015) Zika virus outbreak, Bahia, Brazil. *Emerg. Infect. Dis.*, **21**, 1885–1886.
4. Mlakar,J., Korva,M., Tul,N., Popović,M., Poljšak-Prijatelj,M., Mraz,J., Kolenc,M., Resman Rus,K., Vesnaver Vipotnik,T., Fabjan Vodušek,V., *et al.* (2016) Zika Virus Associated with Microcephaly. *N. Engl. J. Med.*, **374**, 951–958.
5. Beckham,J.D., Pastula,D.M., Massey,A. and Tyler,K.L. (2016) Zika Virus as an Emerging Global Pathogen: Neurological Complications of Zika Virus. *JAMA Neurol.*, 10.1001/jamaneurol.2016.0800.
6. Calvet,G., Aguiar,R.S., Melo,A.S.O., Sampaio,S.A., de Filippis,I., Fabri,A., Araujo,E.S.M., de Sequeira,P.C., de Mendonça,M.C.L., de Oliveira,L., *et al.* (2016) Detection and sequencing of Zika virus from amniotic fluid of fetuses with microcephaly in Brazil: a case study. *Lancet. Infect. Dis.*, **16**, 653–660.
7. Martines,R.B., Bhatnagar,J., Keating,M.K., Silva-Flannery,L., Muehlenbachs,A., Gary,J., Goldsmith,C., Hale,G., Ritter,J., Rollin,D., *et al.* (2016) *Notes from the Field* : Evidence of Zika Virus Infection in Brain and Placental Tissues from Two Congenitally Infected Newborns and Two Fetal Losses — Brazil, 2015. *MMWR. Morb. Mortal. Wkly. Rep.*, **65**, 1–2.
8. Sarno,M., Sacramento,G.A., Khouri,R., do Rosário,M.S., Costa,F., Archanjo,G., Santos,L.A., Nery,N., Vasilakis,N., Ko,A.I., *et al.* (2016) Zika Virus Infection and Stillbirths: A Case of Hydrops Fetalis, Hydranencephaly and Fetal Demise. *PLoS Negl. Trop. Dis.*, **10**, e0004517.
9. Metsky,H.C., Matranga,C.B., Wohl,S., Schaffner,S.F., Freije,C.A., Winnicki,S.M., West,K., Qu,J., Baniecki,M.L., Gladden-Young,A., *et al.* (2017) Zika virus evolution and spread in the Americas. *Nature*, 10.1038/nature22402.
10. Faria,N.R., Quick,J., Claro,I.M., Thézé,J., de Jesus,J.G., Giovanetti,M., Kraemer,M.U.G., Hill,S.C., Black,A., da Costa,A.C., *et al.* (2017) Establishment and cryptic transmission of Zika virus in Brazil and the Americas. *Nature*, 10.1038/nature22401.
11. Grubaugh,N.D., Ladner,J.T., Kraemer,M.U.G., Dudas,G., Tan,A.L., Gangavarapu,K., Wiley,M.R., White,S., Thézé,J., Magnani,D.M., *et al.* (2017) Genomic epidemiology reveals multiple introductions of Zika virus into the United States. *Nature*, 10.1038/nature22400.
12. Liu,Y., Liu,J., Du,S., Shan,C., Nie,K., Zhang,R., Li,X.-F., Zhang,R., Wang,T., Qin,C.-F., *et al.* (2017) Evolutionary enhancement of Zika virus infectivity in Aedes aegypti mosquitoes. *Nature*, **545**, 482–486.
13. Delatorre,E., Mir,D. and Bello,G. (2017) Tracing the origin of the NS1 A188V substitution responsible for recent enhancement of Zika virus Asian genotype infectivity. *Mem Inst Oswaldo Cruz*, 10.1590/0074-02760170299.
14. Davis,B.S., Duggal,N.K., Chang,G.-J.J., Ritter,J.M., McDonald,E.M., Romo,H., Brault,A.C. and Guirakhoo,F. (2017) Differential Neurovirulence of African and Asian Genotype Zika Virus Isolates in Outbred Immunocompetent Mice. *Am. J. Trop. Med. Hyg.*, 10.4269/ajtmh.17-0263.
15. Anfasa,F., Siegers,J.Y., van der Kroeg,M., Mumtaz,N., Stalin Raj,V., de Vrij,F.M.S., Widagdo,W., Gabriel,G., Salinas,S., Simonin,Y., *et al.* (2017) Phenotypic Differences

between Asian and African Lineage Zika Viruses in Human Neural Progenitor Cells. *mSphere*, **2**, e00292-17.
16. Simonin,Y., Loustalot,F., Desmetz,C., Foulongne,V., Constant,O., Fournier-Wirth,C., Leon,F., Molès,J.-P., Goubaud,A., Lemaitre,J.-M., *et al.* (2016) Zika Virus Strains Potentially Display Different Infectious Profiles in Human Neural Cells. *EBioMedicine*, **12**, 161–169.
17. Cugola,F.R., Fernandes,I.R., Russo,F.B., Freitas,B.C., Dias,J.L.M., Guimarães,K.P., Benazzato,C., Almeida,N., Pignatari,G.C., Romero,S., *et al.* (2016) The Brazilian Zika virus strain causes birth defects in experimental models. *Nature*, 10.1038/nature18296.
18. Nowakowski,T.J., Pollen,A.A., Di Lullo,E., Sandoval-Espinosa,C., Bershteyn,M. and Kriegstein,A.R. (2016) Expression Analysis Highlights AXL as a Candidate Zika Virus Entry Receptor in Neural Stem Cells. *Cell Stem Cell*, **18**, 591–596.
19. Quicke,K.M., Bowen,J.R., Johnson,E.L., McDonald,C.E., Ma,H., O'Neal,J.T., Rajakumar,A., Wrammert,J., Rimawi,B.H., Pulendran,B., *et al.* (2016) Zika Virus Infects Human Placental Macrophages. *Cell Host Microbe*, 10.1016/j.chom.2016.05.015.
20. Ginhoux,F., Greter,M., Leboeuf,M., Nandi,S., See,P., Gokhan,S., Mehler,M.F., Conway,S.J., Ng,L.G., Stanley,E.R., *et al.* (2010) Fate mapping analysis reveals that adult microglia derive from primitive macrophages. *Science*, **330**, 841–845.
21. Lum,F.-M., Low,D.K.S., Fan,Y., Tan,J.J.L., Lee,B., Chan,J.K.Y., Rénia,L., Ginhoux,F. and Ng,L.F.P. (2017) Zika Virus Infects Human Fetal Brain Microglia and Induces Inflammation. *Clin. Infect. Dis.*, **64**, 914–920.
22. Ornelas,A.M.M., Pezzuto,P., Silveira,P.P., Melo,F.O., Ferreira,T.A., Oliveira-Szejnfeld,P.S., Leal,J.I., Amorim,M.M.R., Hamilton,S., Rawlinson,W.D., *et al.* (2017) Immune activation in amniotic fluid from Zika virus-associated microcephaly. *Ann. Neurol.*, **81**, 152–156.
23. Tappe,D., Pérez-Girón,J.V., Zammarchi,L., Rissland,J., Ferreira,D.F., Jaenisch,T., Gómez-Medina,S., Günther,S., Bartoloni,A., Muñoz-Fontela,C., *et al.* (2016) Cytokine kinetics of Zika virus-infected patients from acute to reconvalescent phase. *Med. Microbiol. Immunol.*, **205**, 269–273.
24. Manangeeswaran,M., Ireland,D.D.C. and Verthelyi,D. (2016) Zika (PRVABC59) Infection Is Associated with T cell Infiltration and Neurodegeneration in CNS of Immunocompetent Neonatal C57Bl/6 Mice. *PLOS Pathog.*, **12**, e1006004.
25. Galliez,R.M., Spitz,M., Rafful,P.P., Cagy,M., Escosteguy,C., Germano,C.S.B., Sasse,E., Gonçalves,A.L., Silveira,P.P., Pezzuto,P., *et al.* (2016) Zika Virus Causing Encephalomyelitis Associated With Immunoactivation. *Open Forum Infect. Dis.*, **3**, ofw203.
26. Sacramento,C.Q., de Melo,G.R., de Freitas,C.S., Rocha,N., Hoelz,L.V.B., Miranda,M., Fintelman-Rodrigues,N., Marttorelli,A., Ferreira,A.C., Barbosa-Lima,G., *et al.* (2017) The clinically approved antiviral drug sofosbuvir inhibits Zika virus replication. *Sci. Rep.*, **7**, 40920.
27. Bullard-Feibelman,K.M., Govero,J., Zhu,Z., Salazar,V., Veselinovic,M., Diamond,M.S. and Geiss,B.J. (2017) The FDA-approved drug sofosbuvir inhibits Zika virus infection. *Antiviral Res.*, **137**, 134–140.
28. Onorati,M., Li,Z., Liu,F., Sousa,A.M.M., Nakagawa,N., Li,M., Dell'Anno,M.T., Gulden,F.O., Pochareddy,S., Tebbenkamp,A.T.N., *et al.* (2016) Zika Virus Disrupts Phospho-TBK1 Localization and Mitosis in Human Neuroepithelial Stem Cells and Radial Glia. *Cell Rep.*, **16**, 2576–2592.
29. Yanagimachi,M.D., Niwa,A., Tanaka,T., Honda-Ozaki,F., Nishimoto,S., Murata,Y., Yasumi,T., Ito,J., Tomida,S., Oshima,K., *et al.* (2013) Robust and highly-efficient differentiation of functional monocytic cells from human pluripotent stem cells under serum- and feeder cell-free conditions. *PLoS One*, **8**, e59243.
30. Douvaras,P., Sun,B., Wang,M., Kruglikov,I., Lallos,G., Zimmer,M., Terrenoire,C., Zhang,B., Gandy,S., Schadt,E., *et al.* (2017) Directed Differentiation of Human Pluripotent Stem Cells to Microglia. *Stem Cell Reports*, 10.1016/j.stemcr.2017.04.023.

31. Grozdanov,V., Bliederhaeuser,C., Ruf,W.P., Roth,V., Fundel-Clemens,K., Zondler,L., Brenner,D., Martin-Villalba,A., Hengerer,B., Kassubek,J., *et al.* (2014) Inflammatory dysregulation of blood monocytes in Parkinson's disease patients. *Acta Neuropathol.*, **128**, 651–663.
32. Underhill,D.M. (2003) Macrophage recognition of zymosan particles. *J. Endotoxin Res.*, **9**, 176–180.
33. Speert,D.P. and Silverstein,S.C. (1985) Phagocytosis of unopsonized zymosan by human monocyte-derived macrophages: maturation and inhibition by mannan. *J. Leukoc. Biol.*, **38**, 655–658.
34. Ohradanova-Repic,A., Machacek,C., Fischer,M.B. and Stockinger,H. (2016) Differentiation of human monocytes and derived subsets of macrophages and dendritic cells by the HLDA10 monoclonal antibody panel. *Clin. Transl. Immunol.*, **5**, e55.
35. Dang,J., Tiwari,S.K., Lichinchi,G., Qin,Y., Patil,V.S., Eroshkin,A.M. and Rana,T.M. (2016) Zika Virus Depletes Neural Progenitors in Human Cerebral Organoids through Activation of the Innate Immune Receptor TLR3. *Cell Stem Cell*, 10.1016/j.stem.2016.04.014.
36. Garcez,P.P., Nascimento,J.M., de Vasconcelos,J.M., Madeiro da Costa,R., Delvecchio,R., Trindade,P., Loiola,E.C., Higa,L.M., Cassoli,J.S., Vitória,G., *et al.* (2017) Zika virus disrupts molecular fingerprinting of human neurospheres. *Sci. Rep.*, **7**, 40780.
37. Rosenberger,C.M., Podyminogin,R.L., Askovich,P.S., Navarro,G., Kaiser,S.M., Sanders,C.J., McClaren,J.L., Tam,V.C., Dash,P., Noonan,J.G., *et al.* (2014) Characterization of innate responses to influenza virus infection in a novel lung type I epithelial cell model. *J. Gen. Virol.*, **95**, 350–362.
38. Biacchesi,S., Skiadopoulos,M.H., Yang,L., Lamirande,E.W., Tran,K.C., Murphy,B.R., Collins,P.L. and Buchholz,U.J. (2004) Recombinant Human Metapneumovirus Lacking the Small Hydrophobic SH and/or Attachment G Glycoprotein: Deletion of G Yields a Promising Vaccine Candidate. *J. Virol.*, **78**, 12877–12887.
39. Tan,M.C., Battini,L., Tuyama,A.C., Macip,S., Melendi,G.A., Horga,M.A. and Luca Gusella,G. (2007) Characterization of human metapneumovirus infection of myeloid dendritic cells. *Virology*, **357**, 1–9.
40. Bayless,N.L., Greenberg,R.S., Swigut,T., Wysocka,J. and Blish,C.A. (2016) Zika Virus Infection Induces Cranial Neural Crest Cells to Produce Cytokines at Levels Detrimental for Neurogenesis. *Cell Host Microbe*, 10.1016/j.chom.2016.09.006.
41. Tang,H., Hammack,C., Ogden,S.C., Wen,Z., Qian,X., Li,Y., Yao,B., Shin,J., Zhang,F., Lee,E.M., *et al.* (2016) Zika Virus Infects Human Cortical Neural Progenitors and Attenuates Their Growth. *Cell Stem Cell*, **18**, 587–590.
42. Chen,S., Lin,Y., Huang,M., Wu,M., Cheng,S., Lei,H., Lee,C., Chiou,T., Wong,C. and Hsieh,S. (2008) CLEC5A is critical for dengue-virus-induced lethal disease. **453**.
43. Bullard-Feibelman,K.M., Govero,J., Zhu,Z., Salazar,V., Veselinovic,M., Diamond,M.S. and Geiss,B.J. (2017) The FDA-approved drug sofosbuvir inhibits Zika virus infection. *Antiviral Res.*, **137**, 134–140.
44. Garcez,P.P., Loiola,E.C., Madeiro da Costa,R., Higa,L.M., Trindade,P., Delvecchio,R., Nascimento,J.M., Brindeiro,R., Tanuri,A. and Rehen,S.K. (2016) Zika virus impairs growth in human neurospheres and brain organoids. *Science*, 10.1126/science.aaf6116.
45. Qian,X., Nguyen,H.N., Song,M.M., Hadiono,C., Ogden,S.C., Hammack,C., Yao,B., Hamersky,G.R., Jacob,F., Zhong,C., *et al.* (2016) Brain-Region-Specific Organoids Using Mini-bioreactors for Modeling ZIKV Exposure. *Cell*, 10.1016/j.cell.2016.04.032.
46. Wells,M.F., Salick,M.R., Wiskow,O., Ho,D.J., Worringer,K.A., Ihry,R.J., Kommineni,S., Bilican,B., Klim,J.R., Hill,E.J., *et al.* (2016) Genetic Ablation of AXL Does Not Protect Human Neural Progenitor Cells and Cerebral Organoids from Zika Virus Infection. *Cell Stem Cell*, **19**, 703–708.
47. Miller,J.L., deWet,B.J.M., Martinez-Pomares,L., Radcliffe,C.M., Dwek,R. a, Rudd,P.M. and

Gordon,S. (2008) The Mannose Receptor Mediates Dengue Virus Infection of Macrophages. *PLoS Pathog.*, **4**, 11.
48. Meertens,L., Labeau,A., Dejarnac,O., Cipriani,S., Sinigaglia,L., Bonnet-Madin,L., Le Charpentier,T., Hafirassou,M.L., Zamborlini,A., Cao-Lormeau,V.-M., *et al.* (2017) Axl Mediates ZIKA Virus Entry in Human Glial Cells and Modulates Innate Immune Responses. *Cell Rep.*, **18**, 324–333.
49. Chavali,P.L., Stojic,L., Meredith,L.W., Joseph,N., Nahorski,M.S., Sanford,T.J., Sweeney,T.R., Krishna,B.A., Hosmillo,M., Firth,A.E., *et al.* (2017) Neurodevelopmental protein Musashi 1 interacts with the Zika genome and promotes viral replication. *Science (80-.).*
50. Foo,S.-S., Chen,W., Chan,Y., Bowman,J.W., Chang,L.-C., Choi,Y., Yoo,J.S., Ge,J., Cheng,G., Bonnin,A., *et al.* (2017) Asian Zika virus strains target CD14(+) blood monocytes and induce M2-skewed immunosuppression during pregnancy. *Nat. Microbiol.*, 10.1038/s41564-017-0016-3.
51. Haddow,A.D., Schuh,A.J., Yasuda,C.Y., Kasper,M.R., Heang,V., Huy,R., Guzman,H., Tesh,R.B. and Weaver,S.C. (2012) Genetic characterization of Zika virus strains: geographic expansion of the Asian lineage. *PLoS Negl. Trop. Dis.*, **6**, e1477.
52. Mandrekar-Colucci,S. and Landreth,G.E. (2010) Microglia and inflammation in Alzheimer's disease. *CNS Neurol. Disord. Drug Targets*, **9**, 156–167.
53. Rezaie,P., Patel,K. and Male,D.K. (1999) Microglia in the human fetal spinal cord--patterns of distribution, morphology and phenotype. *Brain Res. Dev. Brain Res.*, **115**, 71–81.
54. Aloisi,F. (2001) Immune function of microglia. *Glia*, **36**, 165–179.
55. Lawson,L.J., Perry,V.H., Dri,P. and Gordon,S. (1990) Heterogeneity in the distribution and morphology of microglia in the normal adult mouse brain. *Neuroscience*, **39**, 151–170.
56. Martines,R.B., Bhatnagar,J., de Oliveira Ramos,A.M., Davi,H.P.F., Iglezias,S.D., Kanamura,C.T., Keating,M.K., Hale,G., Silva-Flannery,L., Muehlenbachs,A., *et al.* (2016) Pathology of congenital Zika syndrome in Brazil: a case series. *Lancet (London, England)*, **388**, 898–904.
57. Yuki,N. and Hartung,H.-P. (2012) Guillain-Barré syndrome. *N. Engl. J. Med.*, **366**, 2294–304.
58. Marchetto,M.C.N., Carromeu,C., Acab,A., Yu,D., Yeo,G.W., Mu,Y., Chen,G., Gage,F.H. and Muotri,A.R. (2010) A model for neural development and treatment of Rett syndrome using human induced pluripotent stem cells. *Cell*, **143**, 527–539.
59. Nageshappa,S., Carromeu,C., Trujillo,C.A., Mesci,P., Espuny-Camacho,I., Pasciuto,E., Vanderhaeghen,P., Verfaillie,C.M., Raitano,S., Kumar,A., *et al.* (2015) Altered neuronal network and rescue in a human MECP2 duplication model. *Mol. Psychiatry*, 10.1038/mp.2015.128.
60. Griesi-Oliveira,K., Acab,A., Gupta,A.R., Sunaga,D.Y., Chailangkarn,T., Nicol,X., Nunez,Y., Walker,M.F., Murdoch,J.D., Sanders,S.J., *et al.* (2014) Modeling non-syndromic autism and the impact of TRPC6 disruption in human neurons. *Mol. Psychiatry*, 10.1038/mp.2014.141.

Figure 1

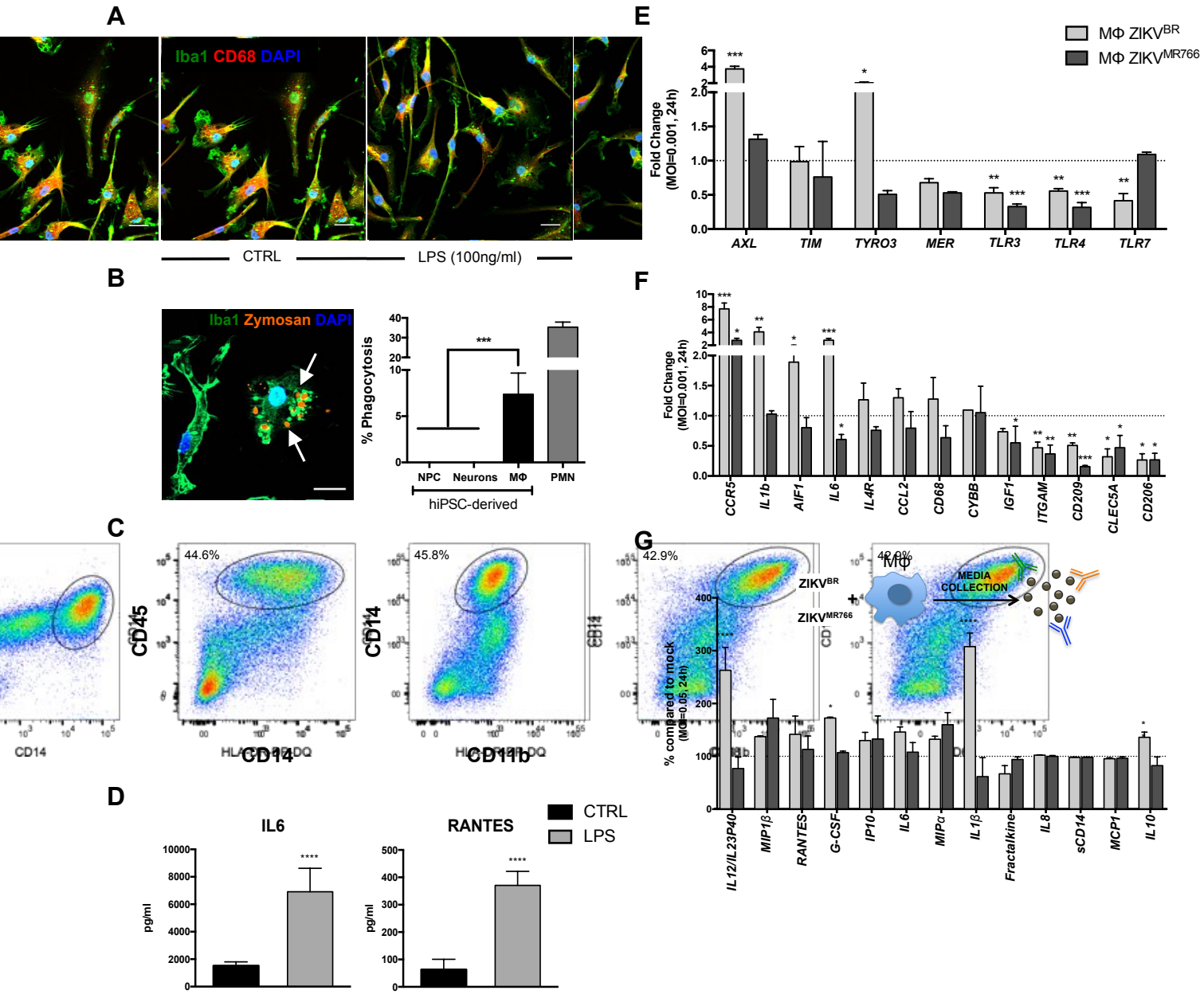
A
Iba1 CD68 DAPI
CTRL
LPS (100ng/ml)
B
Iba1 Zymosan DAPI
% Phagocytosis
NPC
Neurons
MΦ
PMN
hiPSC-derived
C
CD45
CD14
44.6%
45.8%
CD11b
D
IL6
RANTES
CTRL
LPS
pg/ml
E
MΦ ZIKV^BR
MΦ ZIKV^MR766
Fold Change (MOI=0.001, 24h)
AXL
TIM
TYRO3
MER
TLR3
TLR4
TLR7
F
CCR5
IL1b
AIF1
IL6
IL4R
CCL2
CD68
CYBB
IGF1
ITGAM
CD209
CLEC5A
CD206
G
42.9%
ZIKV^BR
ZIKV^MR766
MΦ
MEDIA COLLECTION
% compared to mock (MOI=0.05, 24h)
IL12/IL23P40
MIP1β
RANTES
G-CSF
IP10
IL6
MIPα
IL1β
Fractalkine
IL8
sCD14
MCP1
IL10

Figure 2

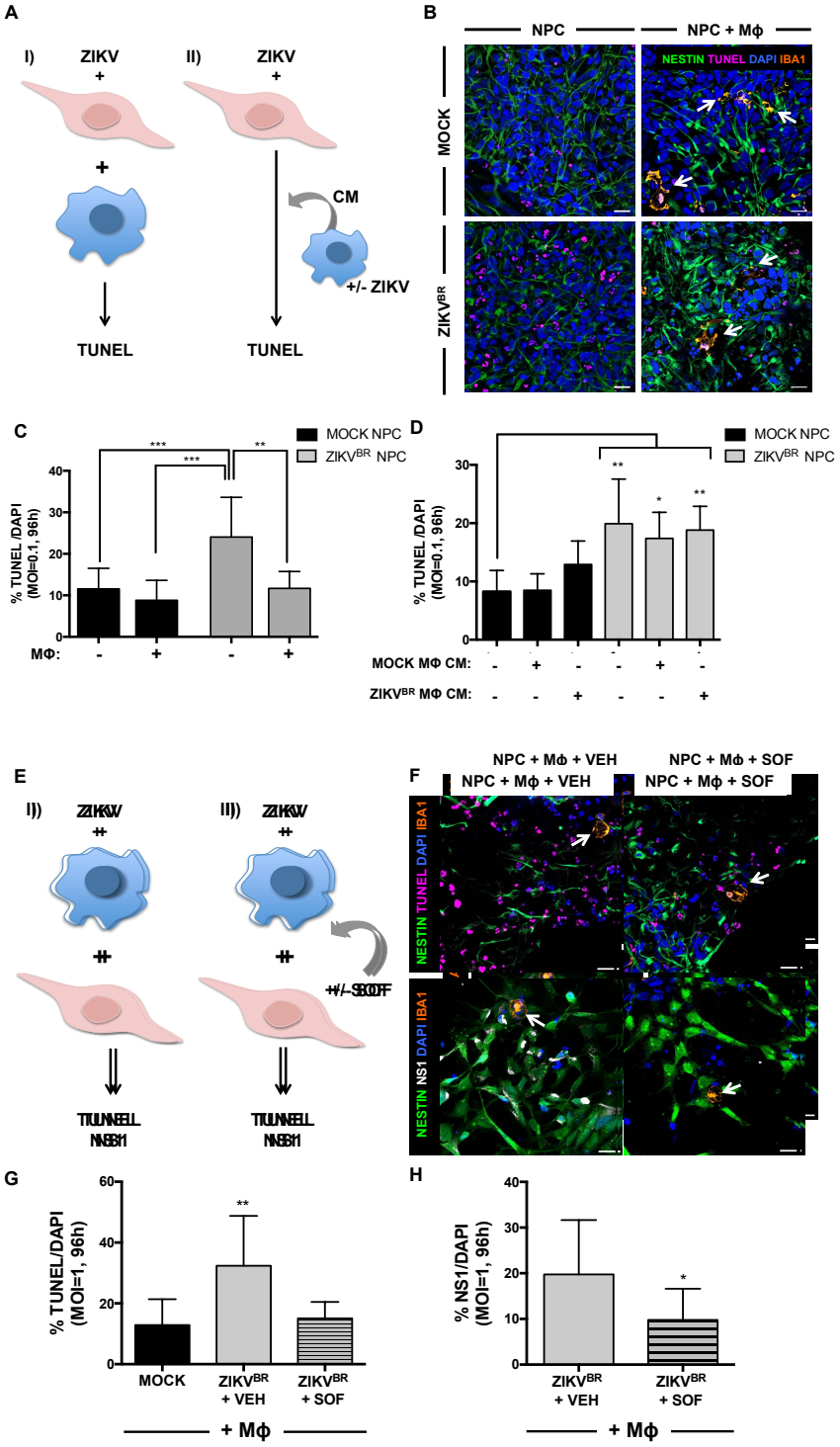
A
I) ZIKV +
II) ZIKV +
CM
+/- ZIKV
TUNEL
TUNEL
B
NPC
NPC + Mϕ
MOCK
ZIKVBR
NESTIN TUNEL DAPI IBA1
C
MOCK NPC
ZIKVBR NPC
% TUNEL /DAPI (MOI=0.1, 96h)
MΦ:
D
MOCK NPC
ZIKVBR NPC
% TUNEL /DAPI (MOI=0.1, 96h)
MOCK MΦ CM:
ZIKVBR MΦ CM:
E
I))
III))
+/- SOF
TUNEL
NS1
F
NPC + Mϕ + VEH
NPC + Mϕ + SOF
NESTIN TUNEL DAPI IBA1
NESTIN NS1 DAPI IBA1
G
% TUNEL/DAPI (MOI=1, 96h)
MOCK
ZIKVBR + VEH
ZIKVBR + SOF
+ Mϕ
H
% NS1/DAPI (MOI=1, 96h)
ZIKVBR + VEH
ZIKVBR + SOF
+ Mϕ

Figure S1

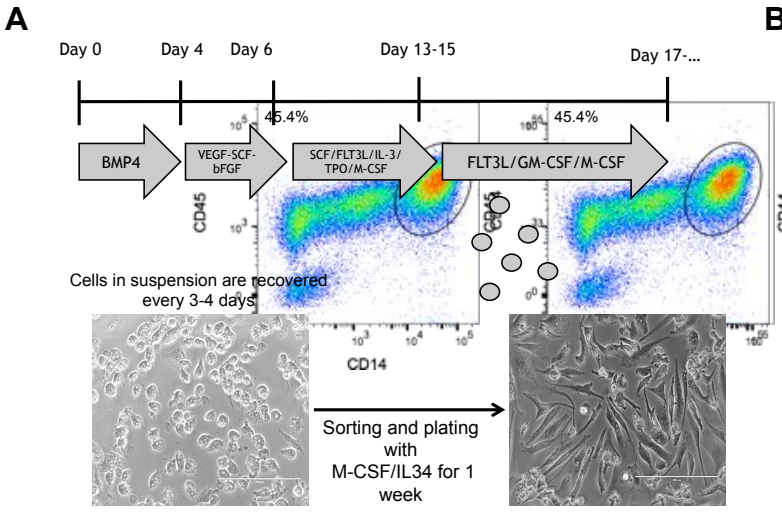
A
Day 0
Day 4
Day 6
Day 13-15
Day 17-...
BMP4
VEGF-SCF-bFGF
SCF/FLT3L/IL-3/TPO/M-CSF
FLT3L/GM-CSF/M-CSF
45.4%
45.4%
CD45
CD14
Cells in suspension are recovered every 3-4 days
Sorting and plating with M-CSF/IL34 for 1 week

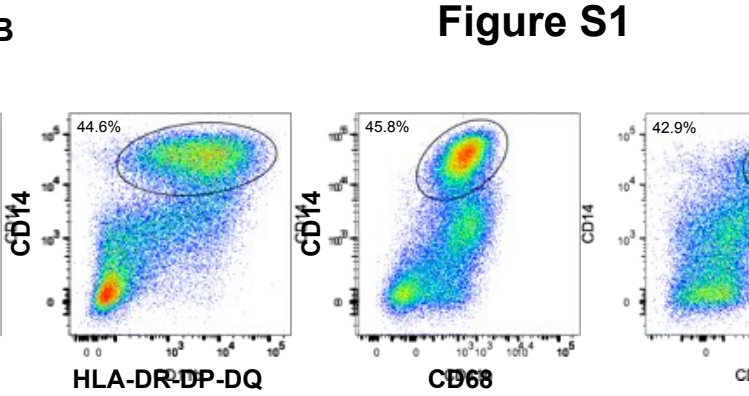
B
44.6%
45.8%
42.9%
CD14
HLA-DR-DP-DQ
CD68

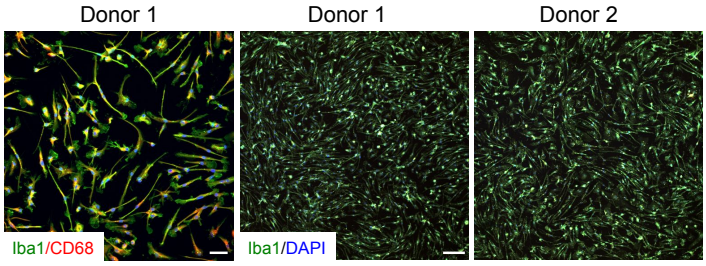
C
Donor 1
Donor 1
Donor 2
Iba1/CD68
Iba1/DAPI

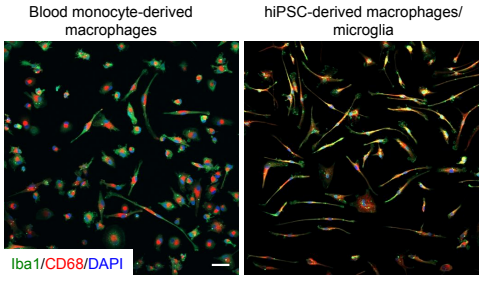
D
Blood monocyte-derived macrophages
hiPSC-derived macrophages/ microglia
Iba1/CD68/DAPI

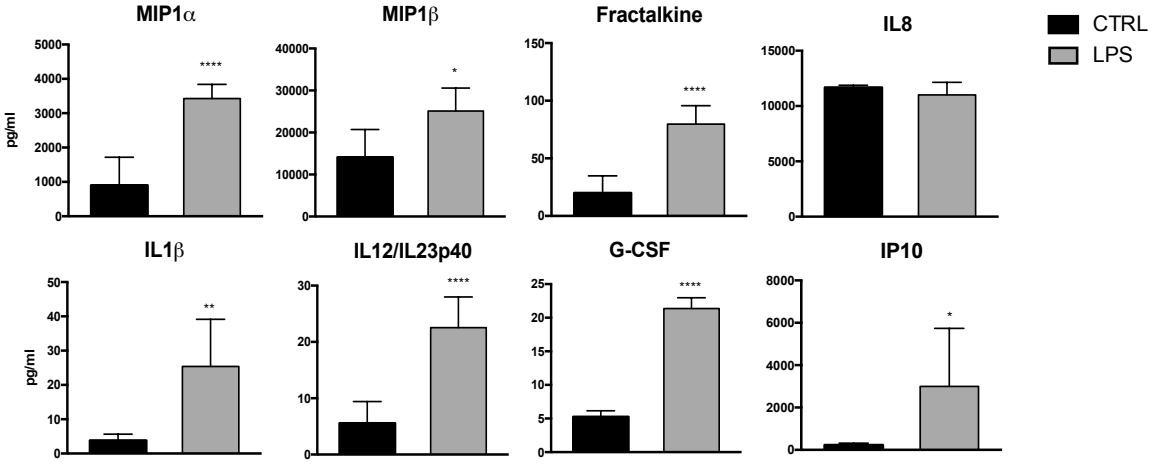
E
MIP1α
MIP1β
Fractalkine
IL8
IL1β
IL12/IL23p40
G-CSF
IP10
pg/ml
CTRL
LPS

Figure S2

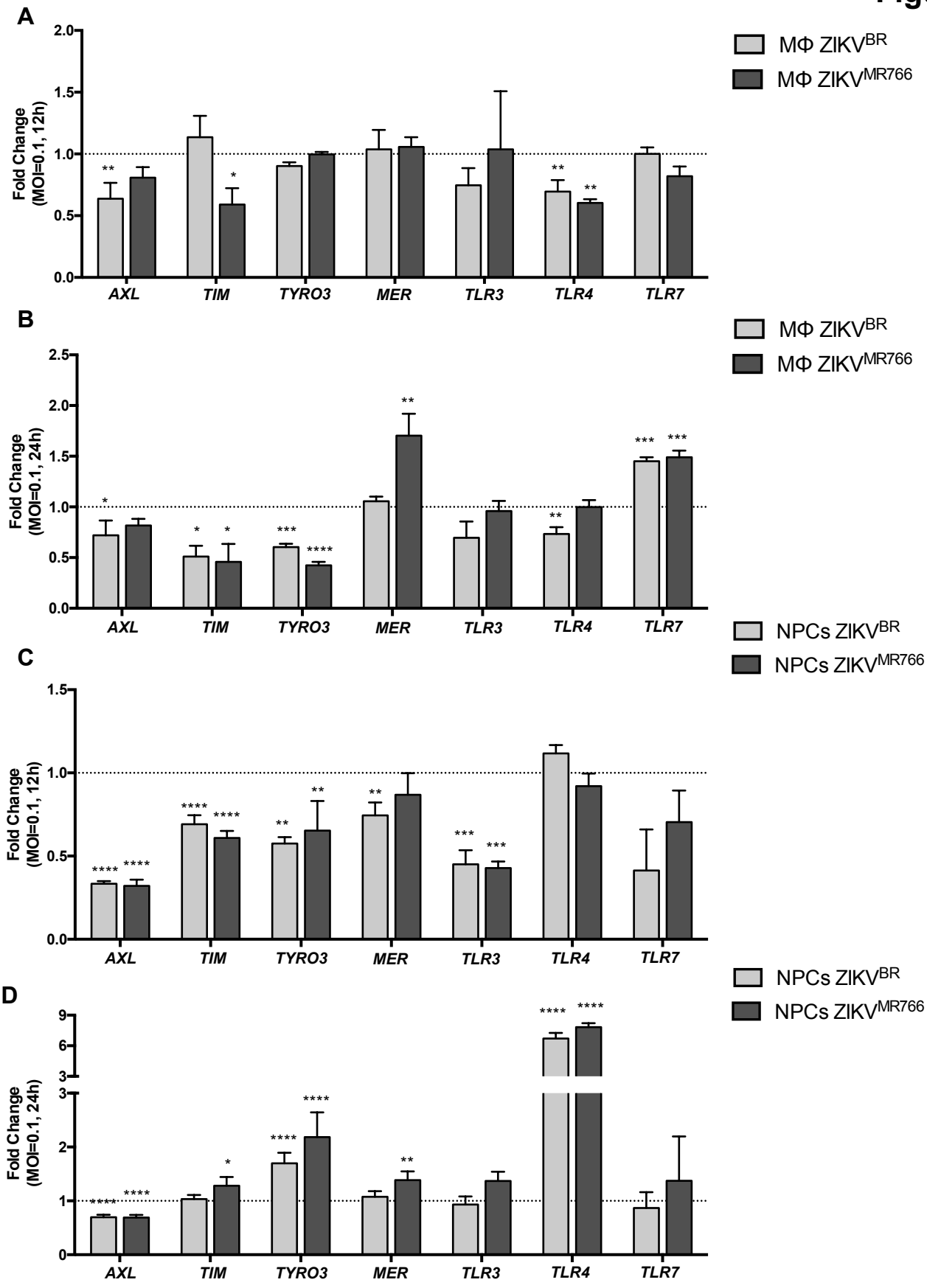
A
Fold Change (MOI=0.1, 12h)
2.0
1.5
1.0
0.5
0.0
AXL
TIM
TYRO3
MER
TLR3
TLR4
TLR7
MΦ ZIKV^BR
MΦ ZIKV^MR766
B
Fold Change (MOI=0.1, 24h)
2.5
2.0
1.5
1.0
0.5
0.0
AXL
TIM
TYRO3
MER
TLR3
TLR4
TLR7
MΦ ZIKV^BR
MΦ ZIKV^MR766
C
Fold Change (MOI=0.1, 12h)
1.5
1.0
0.5
0.0
AXL
TIM
TYRO3
MER
TLR3
TLR4
TLR7
NPCs ZIKV^BR
NPCs ZIKV^MR766
D
Fold Change (MOI=0.1, 24h)
9
6
3
3
2
1
0
AXL
TIM
TYRO3
MER
TLR3
TLR4
TLR7
NPCs ZIKV^BR
NPCs ZIKV^MR766

Figure S3

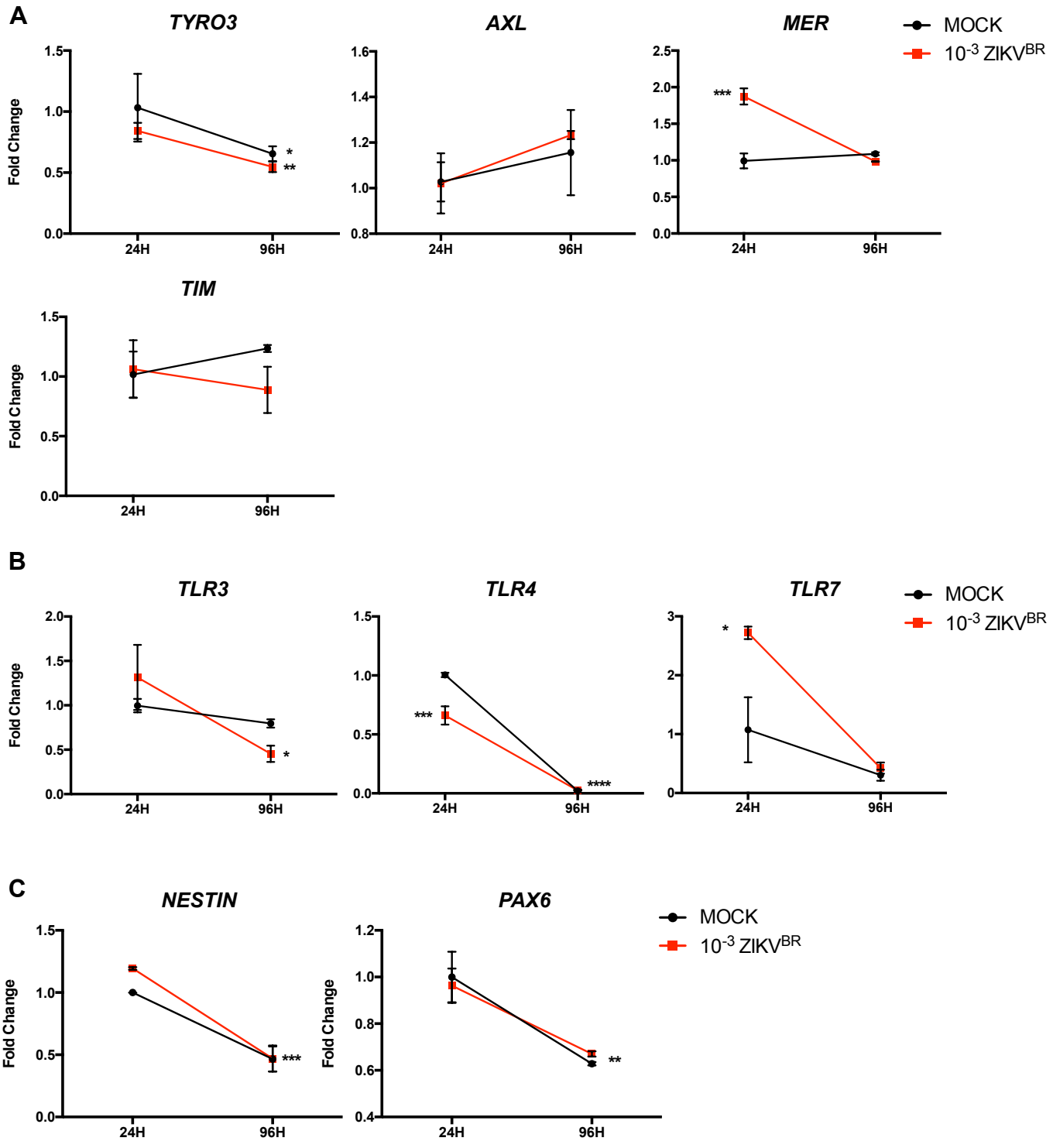
A
TYRO3
AXL
MER
TIM
Fold Change
24H
96H
MOCK
10-3 ZIKVBR
B
TLR3
TLR4
TLR7
C
NESTIN
PAX6

Figure S4

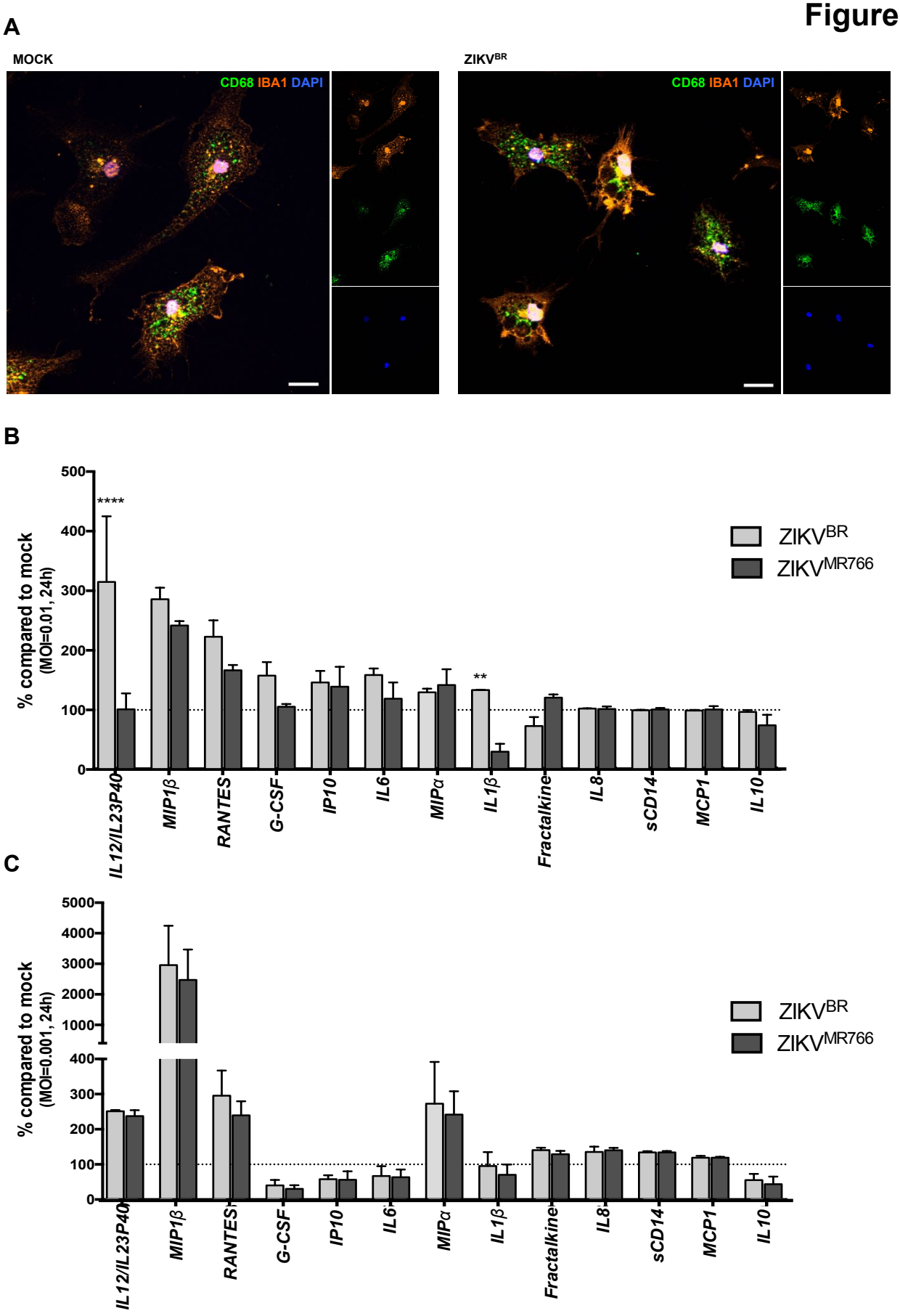
A
MOCK
CD68 IBA1 DAPI
ZIKV^BR
CD68 IBA1 DAPI
B
% compared to mock
(MOI=0.01, 24h)
ZIKV^BR
ZIKV^MR766
****
**
IL12/IL23P40
MIP1β
RANTES
G-CSF
IP10
IL6
MIPα
IL1β
Fractalkine
IL8
sCD14
MCP1
IL10
C
% compared to mock
(MOI=0.001, 24h)
ZIKV^BR
ZIKV^MR766
IL12/IL23P40
MIP1β
RANTES
G-CSF
IP10
IL6
MIPα
IL1β
Fractalkine
IL8
sCD14
MCP1
IL10

Figure S5

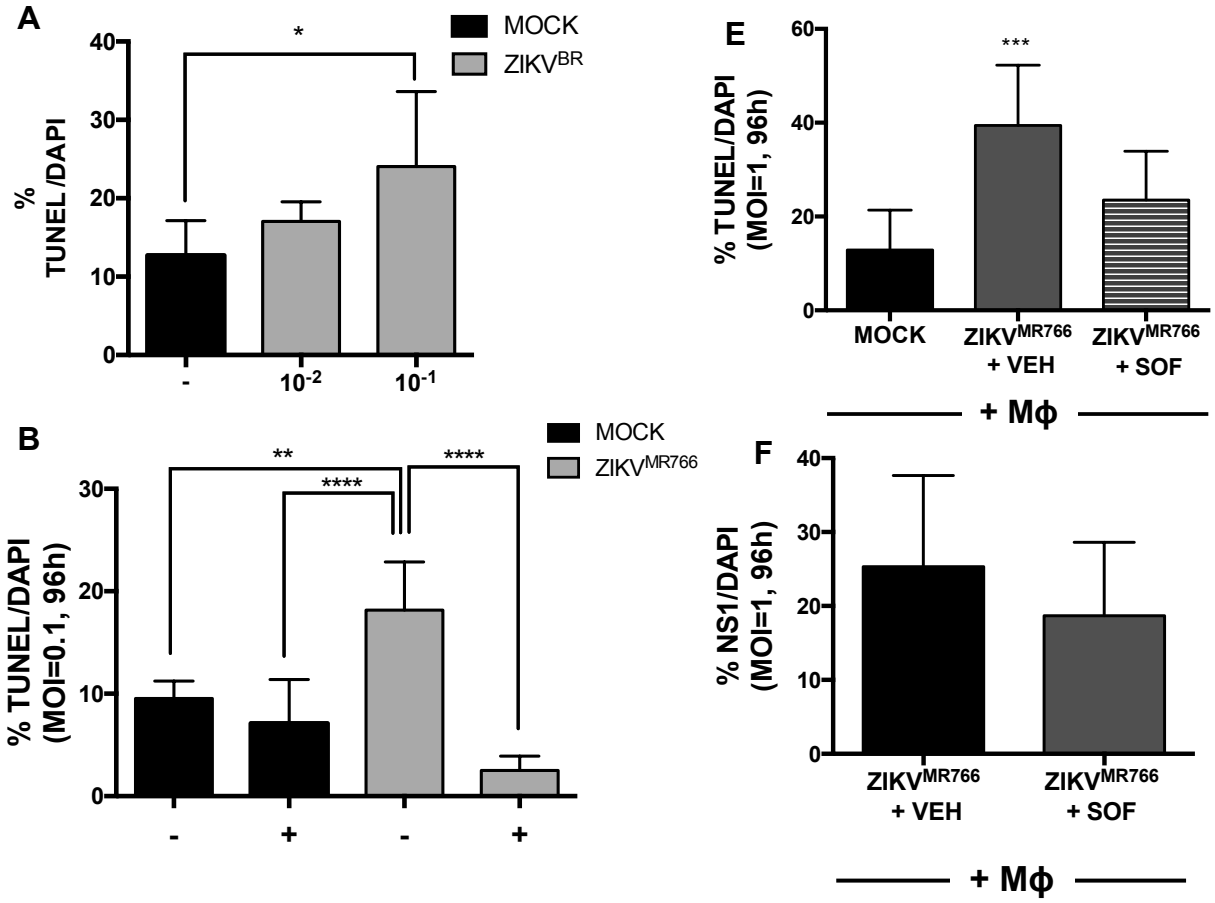

C

% Mϕ/NPC	Mean±SD (%)	p-value
Mock	2.195 ± 0.103	p=0.4766
ZIKV^{BR}	1.833 ± 0.793	

D

Mϕ in apoptosis	Mean±SD (%)	p-value
Mock	2.982 ± 3.619	p=0.4638
ZIKV^{BR}	1.693 ± 2.020	